Science of the Total Environment 733 (2020) 139212

Contents lists available at ScienceDirect

Science of the Total Environment

journal homepage: www.elsevier.com/locate/scitotenv

Time resolved data unveils the complex DOM dynamics in a Mediterranean river

Simona Retelletti Brogi [a,*], Cecilia Balestra [b], Raffaella Casotti [b], Gianpiero Cossarini [c], Yuri Galletti [a], Margherita Gonnelli [a], Stefano Vestri [a], Chiara Santinelli [a]

[a] Istituto di Biofisica, CNR, Via G. Moruzzi, Pisa 56124, Italy
[b] Stazione Zoologica Anton Dohrn, Villa Comunale, Naples 80121, Italy
[c] Istituto Nazionale di Oceanografia e Geofisica Sperimentale (OGS), Borgo Grotta Gigante 42/C, 34010 Sgonico, (TS), Italy

HIGHLIGHTS

- River seasonal dynamics: from winter terrestrial to summer autochthonous FDOM
- 80% of the DOC flux is delivered to the coastal area during the autumn/winter.
- 1/4 of the annual DOC flux transported to coastal areas by single large flood events.

GRAPHICAL ABSTRACT

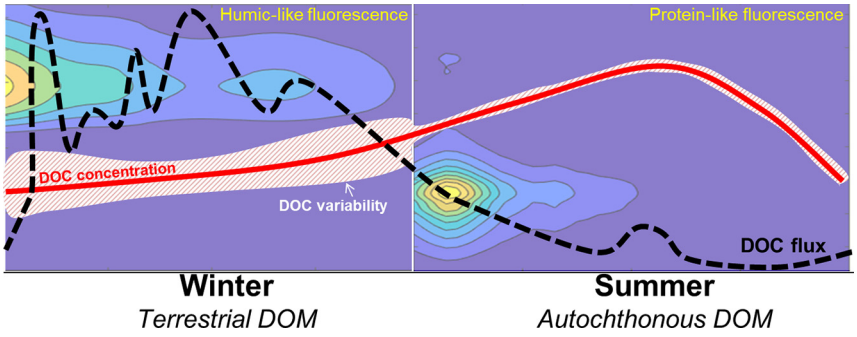

ARTICLE INFO

Article history:
Received 17 February 2020
Received in revised form 2 May 2020
Accepted 2 May 2020
Available online 06 May 2020

Editor: Dr. Damia Barcelo

Keywords:
DOM
DOC
Arno
River
Carbon fluxes
FDOM
Floods

ABSTRACT

In this study, dissolved organic carbon (DOC) data and optical properties (absorbance and fluorescence) of DOM, weekly collected in the Arno River for 2 years, are used to investigate the main processes determining DOM temporal dynamics in a small Mediterranean river, with torrential hydrology and medium-high human impact, and to quantify the contribution of this river to Med Sea carbon budget. A clear seasonal cycle of DOM, with DOC values ranging between 170 and 490 μM, was observed. Optical properties indicates that DOM quality in the river is different depending on the season; terrestrial humic-like substances prevail in winter, when discharge and floods are the main drivers of DOM concentration and quality, whereas autochthonous protein-like substances prevail in spring and summer, when biological processes dominate.

Our results provide a robust estimate of the DOC flux to the Med Sea ($9.6 \cdot 10^9$ g DOC yr^{-1}) and of its range of variability ($12.95 \cdot 10^9$–$5.12 \cdot 10^9$ g DOC yr^{-1}). The 80% of this flux was generally delivered during autumn/winter with significant amounts ascribed to single flood events (up to 26% in 2014).

This study, by providing a rich dataset on water quantity and quality and by quantifying the importance of the hydrological regime on DOC transport, represents an important step toward a quantitative modeling of the Arno River.

* Corresponding author.
E-mail address: Simona.retelletti@pi.ibf.cnr.it (S. Retelletti Brogi).

https://doi.org/10.1016/j.scitotenv.2020.139212
0048-9697/

1. Introduction

The importance of riverine dissolved organic matter (DOM) in the marine ecosystem is widely recognized, being the primary source of reduced carbon to the coastal environment (Raymond and Spencer, 2015), controlling the functioning of the microbial food web (Crump et al., 2009) and the bioavailability of metals and other toxic compounds (Aiken et al., 2011). In rivers, DOM dynamics is determined by the interactions between the biological processes (biosphere), the inputs from the land (lithosphere), the weather and atmospheric inputs (atmosphere) and human activities (antroposphere), as well by physico-chemical modifications within the river itself. Riverine DOM originates from autochthonous (phytoplankton, aquatic plants, heterotrophs) and allochthonous (soil leaching, rocks weathering, atmospheric inputs) sources, as well as by anthropic activities (industries, wastewaters, intense agriculture and breeding farms) (Del Giorgio and Pace, 2008; Elliott et al., 2006; Fasching et al., 2014; Fisher et al., 2004; Griffith and Raymond, 2011). Before reaching the coastal area, DOM undergoes several modifications due to photodegradation (Meng et al., 2013; Opsahl and Benner, 1998; Shiller et al., 2006; Xie et al., 2004), flocculation (Asmala et al., 2014), and/or removal and transformation by heterotrophs (Fasching et al., 2014; Findlay, 2010; Retelletti Brogi et al., 2015). These processes determine the dynamics of DOM in the rivers and have a strong impact on the quantity and quality of DOM reaching the sea and therefore on the release and/or sequestration of CO_2 at the river mouth (Battin et al., 2008; Bianchi et al., 2013). In the last decades, a big effort has been done in order to characterize riverine DOM (Nebbioso and Piccolo, 2013; Sleighter and Hatcher, 2008; Spencer et al., 2012; Ward et al., 2013) and to estimate global riverine carbon fluxes (Cauwet, 2002; Dai et al., 2012; Ludwig and Probst, 1996). Many studies focused on the impact of floods and extreme events (Bianchi et al., 2013; Hitchcock and Mitrovic, 2015; Raymond et al., 2016; Wagner et al., 2019; Zuijdgeest et al., 2016) because of the expected increase of such events due to climate change and the impact they have on the global carbon cycle (Reichstein et al., 2013; Yi et al., 2015).

In the Mediterranean Sea (Med Sea), the riverine contribution to the total DOM pool is expected to be particularly relevant because of its long coastline ($46 \cdot 10^3$ km), high population density along the coasts, and its small size. However, when the riverine dissolved organic carbon (DOC) fluxes are divided by the total water volume of the Med Sea, the estimated flux ($0.17–0.19 \cdot 10^6$ g DOC yr^{-1} km^{-3}) (Santinelli, 2015) is comparable to values estimated for the oceans ($0.14–0.18 \cdot 10^6$ g DOC yr^{-1} km^{-3}) (Cauwet, 2002; Dai et al., 2012). Only a few studies report DOM dynamics in Mediterranean rivers (Berto et al., 2010; Butturini et al., 2016; Gómez-Gutiérrez et al., 2006; Gonnelli et al., 2013; Kaiser et al., 2004; Louis et al., 2009; Panagiotopoulos et al., 2012; Para et al., 2010; Pettine et al., 1998; Retelletti Brogi et al., 2015; Sempéré et al., 2000; Vignudelli et al., 2004); among these, only 5 studied DOM temporal variability in the Po, Rhone, and Tagliamento rivers (Berto et al., 2010; Kaiser et al., 2004; Panagiotopoulos et al., 2012; Pettine et al., 1998; Sempéré et al., 2000). These studies focused mostly on DOC concentration, whereas, to the best of the author's knowledge, there is no study reporting temporal variability of DOM quality in any Mediterranean river.

The optical properties (absorption and fluorescence) of the chromophoric and fluorescent fractions of DOM (CDOM and FDOM) can track changes in DOM quality by providing information on its main sources, redox state, biological reactivity and molecular weight (Fellman et al., 2010; Miller et al., 2009; Mladenov et al., 2008; Weishaar et al., 2003). Being rapid, cheap and requiring minor sample pre-treatment (only filtration), these techniques allow for extensive sampling programs (Jaffé et al., 2008), helping in the identification of the main processes driving DOM variability.

This study aims at investigating the main processes affecting DOM temporal dynamics in the lower part of the Arno River before mixing with the seawater, and to give a robust estimate of the contribution of Arno River to DOC fluxes to the Med Sea.

Considering the total Mediterranean Sea water discharge budget (van Apeldoorn and Bouwman, 2012), only 5 rivers have a discharge higher than 300 m^3 s^{-1} (41% of the total discharge), 10 rivers have a medium discharge (150–300 m^3 s^{-1}, that is 16% of the total) and 87 rivers are small (discharge 15–150 m^3 s^{-1}, that is 29% of the total) as the Arno River (86 m^3 s^{-1}). The Arno River is characterized by a typical torrential hydrological regime as indicated by the high annual variability in discharge and frequent flooding during high rain periods (Caporali et al., 2005; Regional Hydrological Service database, www.sir.toscana.it). It features high DOC concentration (Retelletti Brogi et al., 2015; Santinelli, 2015), due to the medium-high anthropic impact along its course. As a matter of fact, according to the EU statistics (EU statistics, 2015), the Tuscany region has a higher values of artificial land cover (40.3%) with respect to the EU28 average (36.3%). In this study, the Arno River was therefore considered as a case study for DOM dynamics in small Mediterranean rivers with torrential hydrology and medium-high human impact.

2. Methods

2.1. Characterization of the study area

The Arno River rises within the Mt. Falterona (1358 m above sea level) in the northern Apennines and reaches the Tyrrhenian Sea, covering a total length of 241 km with an average elevation of 353 m above sea level and an average discharge of 82.44 m^3 s^{-1}. With a drainage basin of 8228 km^2it is the 5th Italian river for basin extension. The basin is mostly characterized by hilly area (>70%, Fig. S1). Most of the geological formations (>95%) are characterized by low permeability (i.e. clay, marl, schist, sandstones) making the discharge influenced mostly by the precipitations, detailed information on the river lithology and mineralogy can be found in Cortecci et al. (2009) and Dinelli et al. (2005). The basin is located in the temperate climatic zone, with temperature gradually increasing between January and July/August and gradually decreasing afterwards until the end of the year. Between January and May, there are regular and abundant rainfalls, whereas heavy rainfalls are unevenly distributed between October and December (Arno River Basin Authority, www.adbarno.it, accessed on 27.03.2020). Along its course, the Arno River flows through several cities, the biggest being Arezzo, Firenze and Pisa (approximately 99.5, 379.5 and 90.5 thousand inhabitants, respectively). It is also affected by several human activities such as large agricultural sites, covering 50% of the basin area (Fig. 1), and industries such as paper-mills, tanneries, textile industries and electrochemical plants (Cortecci et al., 2009).

2.2. Sampling site and samples collection

Water samples were weekly collected in the morning (between 9:00 a.m. and 1:00 p.m.), from January 2014 to December 2015 in the Arno River at one station located in Pisa (Fig. 1, 43.71°N; 10.40°E), 12 km inside the river mouth. This location was chosen because it is close to the river mouth, but far enough from the estuary to be not influenced by the seawater. In addition, there is no any other input after this location, neither tributaries nor significant anthropogenic activities. Additional high frequency samples (i.e., 6, 12 and 24 h) were collected during a flood event in February 2016 and are used to assess the uncertainty of the DOC transport computation during the floods.

Temperature and conductivity were measured by a portable Hanna 9033 conductivity probe (Hanna Instruments Inc., USA). Daily average river discharge and precipitation are available from the Regional Hydrological Service (www.sir.toscana.it). Precipitation data from 2002 to 2019 for 122 meteorological stations were collected and averaged to provide the precipitation time-series over the Arno drainage basin. The meteorological stations used to retrieve precipitation records

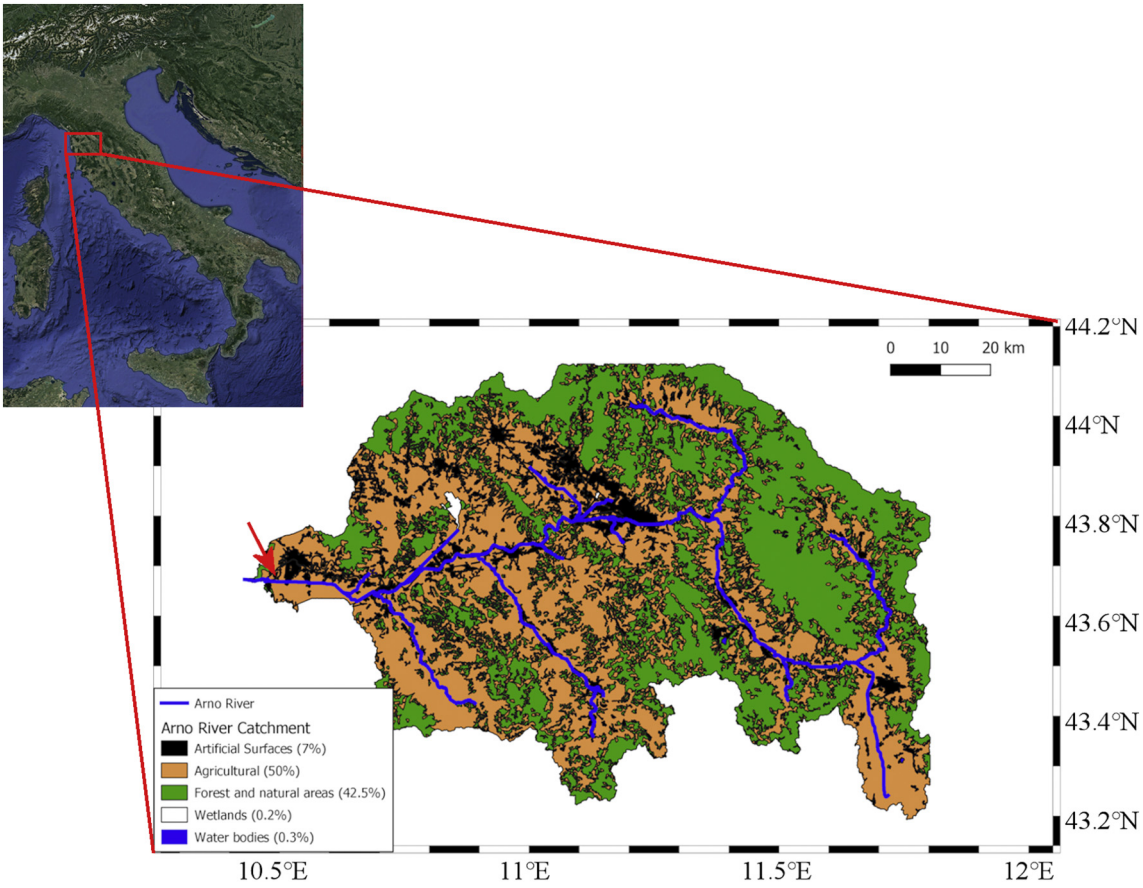

Fig. 1. Arno River basin location and land cover characterization. The land cover data were derived from the CORINE Land Cover 2018 (CLC 2018) database and the land cover map produced by using QGIS software. The red star indicates the location of the sampling station. (For interpretation of the references to color in this figure legend, the reader is referred to the web version of this article.)

cover almost uniformly the plain, hill and mountain areas of the Arno drainage basin, and daily averages were computed for spatial coverage higher than 90% ensuring that the average is a good estimation of the water input to the Arno River during flood periods.

To avoid resuspension from the riverbanks, surface water was collected in the center of the river from a bridge using a cylindrical, 1 l, acid-washed Teflon sampler. This sampler was specifically designed in our laboratory by Stefano Vestri and realized by Edi Progetti Srl (Pontedera, Pisa) and was optimized to collect surface water. Samples were collected within the upper 1 m to avoid the interference with the bottom saltwater intrusion. The salinity (derived from the conductivity measurement) of the collected samples was always <0.5. Detailed information on the sampling and environmental conditions is given in Table S1.

Samples for DOC, CDOM and FDOM analyses were collected into 2 l, acid-washed, polycarbonate bottles (Nalgene) and kept refrigerated and in the dark. Once in the lab (maximum 1 h from the sampling), samples were filtered through a 0.2 μm pore size filter (Whatman Polycap, 6705–3602 capsules) and dispensed into 3 × 60 ml acid-washed polycarbonate (Nalgene) bottles, used as analytical replicates. DOC, CDOM, and FDOM were immediately measured after filtration.

2.3. Dissolved organic carbon (DOC) concentration

DOC was measured by high-temperature catalytic oxidation using a Shimadzu Total Organic Carbon analyzer (TOC-Vcsn) following the method reported by (Santinelli et al., 2015). The instrument performance was verified by comparison with DOC Consensus Reference Waters (Hansell, 2005) (CRM Batch #13 nominal concentration of 41–44 μM; measured concentration 42.3 ± 0.9 μM, $n = 88$). The results are shown as the average and standard deviation of 3 analytical replicates.

2.4. DOM optical properties: absorption and fluorescence (CDOM and FDOM)

Absorbance spectra (230 to 700 nm) were measured using a Jasco UV–visible spectrophotometer (Mod-7850) equipped with a 10 cm quartz cuvette, following the method reported by Retelletti Brogi et al. (2015). Absorbance spectra were elaborated by using the ASFit tool (Omanović et al., 2019). Absorption coefficients were calculated at 254 (a_{254}) and 440 nm (a_{440}). The Specific Ultraviolet Absorption coefficient ($SUVA_{254}$) was calculated as the ratio between a_{254} and DOC concentration (Weishaar et al., 2003).

Fluorescence excitation-emission Matrixes (EEMs) were obtained using the Aqualog spectrofluorometer (Horiba) with a 10 × 10 mm quartz cuvette. Excitation ranged between 250 and 450 nm at 5 nm increment, emission was recorded between 212 and 620 nm every 0.8 nm with an integration time of 5 s. The EEMs were subtracted by the EEM of Milli-Q water and corrected for the inner-filter effect (Lakowicz, 2006). Rayleigh and Raman scatter peaks were removed by using the monotone cubic interpolation (shape-preserving) (Carlson and Fritsch, 1989) and EEMs were normalized by the integrated Raman band of Milli-Q water (λ_{ex} = 350 nm; λ_{ex} = 371–428 nm; Lawaetz and Stedmon, 2009). Fluorescence intensities are therefore reported as Raman Units (R.U.). PARAllel FACtor analysis (PARAFAC, drEEM Toolbox, Murphy et al., 2013) was carried out on the EEMs and resulted in a 5-component model (Fig. 6, Table S2). The validation of the PARAFAC model was performed by visual inspection of the residuals, split-half analysis and percentage of explained variance (99.5%). The

relative contribution of each component (%C) was calculated as the percentage of each component on the total fluorescence (sum of all the 5 components in each sample).

2.5. Heterotrophic prokaryotes abundance (HPA)

Samples for Heterotrophic Prokaryotes Abundance (HPA) were fixed for 10 min with a mix of paraformaldehyde (PF, 1%) and glutaraldehyde (GL, 0.05%), frozen in liquid N_2 and stored at −80 °C until the analysis. Once thawed, samples were stained with SYBR Green (Invitrogen Milan, Italy) 10^{-3} dilution of stock solution for 15 min at room temperature. Heterotrophic prokaryotes (HP) cell concentrations were estimated using a FACSVerse flow cytometer (BD BioSciences Inc., Frankyn Lakes, USA) equipped with a 488 nm Ar laser and standard filter set. Data analysis was performed using the FCS Express software and HP discriminated from other particles based on scatter and green fluorescence from SYBR Green (Balestra et al., 2011).

2.6. Statistics

Linear, logarithmic, power law regression analysis and Pearson correlation analysis between the variables were computed using Sigma Plot (Systat Softwares Inc., USA) and Origin (OriginLab Co., USA) software and considered significant for $p < .05$ (t-test).

3. Results

3.1. Arno River discharge and temperature

Discharge ranged from 13 to 1806 $m^3\ s^{-1}$ in 2014 (average 138 $m^3\ s^{-1}$) and from 7 to 629 $m^3\ s^{-1}$ in 2015 (average 50 $m^3\ s^{-1}$). It is noteworthy that these values well represent the high variability of the Arno River discharge. If the data recorded in the last 17 years are taken into consideration (validated discharge data from the hydrological regional service, www.sir.toscana.it, between 2001 and 2018), 2014 has the second highest discharge, whereas the 2015 has the second to last discharge (Fig. S1) in agreement with the different precipitation regimes in the two years compared to the climatology (Fig. 2). The Arno water discharge regime reflects the succession of raining and dry seasons in the region, and a rapid response of discharge peaks was generally observed after relevant precipitation events (Fig. 2).

In order to investigate the importance of the hydrological regime to the annual DOC transport, flood events were identified by daily discharge higher than 250 $m^3\ s^{-1}$ (i.e., ~3 times the annual mean river discharge of the last 18 years) lasting for at least 3 consecutive days. Eight flood events were recorded (Table 1), showing the very high interannual variability between the two investigated years. Large and intermediate flood events, with typical return period of 4.5 and 1.5 years, were recorded in 2014, whereas only small flood events (Table 1) and minor peaks in discharge were observed in February, March and late October 2015 (Fig. 2 and Table 1).

The temperature in the river ranged between 7 °C and 27 °C in 2014 and between 4 °C and 32 °C in 2015 (Fig. 2). In 2014, the temperature increased constantly from January to mid-June, it ranged between 23 and 27 °C from mid-June until the end of August and then it decreased until the end of the year. In 2015, the temperature kept increasing to reach its maximum on July 24th.

3.2. Heterotrophic prokaryotes abundance

HPA ranged between $0.72 \cdot 10^6$ and $7.8 \cdot 10^6$ cells ml^{-1} in 2014 and between $0.74 \cdot 10^6$ and $9.6 \cdot 10^6$ cells ml^{-1} in 2015. High Nucleic Acid (HNA; Bouvier et al., 2007; Fig. S3) accounted for >50% of total counts in all the samples. In both years, HPA showed variable but low values until May, when an increase was observed (Fig. 3). In 2014, values were almost constant until August, followed by a sharp peak ($7.8 \cdot 10^6$ cells ml^{-1}), whereas in 2015, HPA increased constantly from May to July, when the highest value was observed ($9.6 \cdot 10^6$ cells ml^{-1}). In both years, after the peak, HPA markedly decreased, with values never rising again till the end of the year.

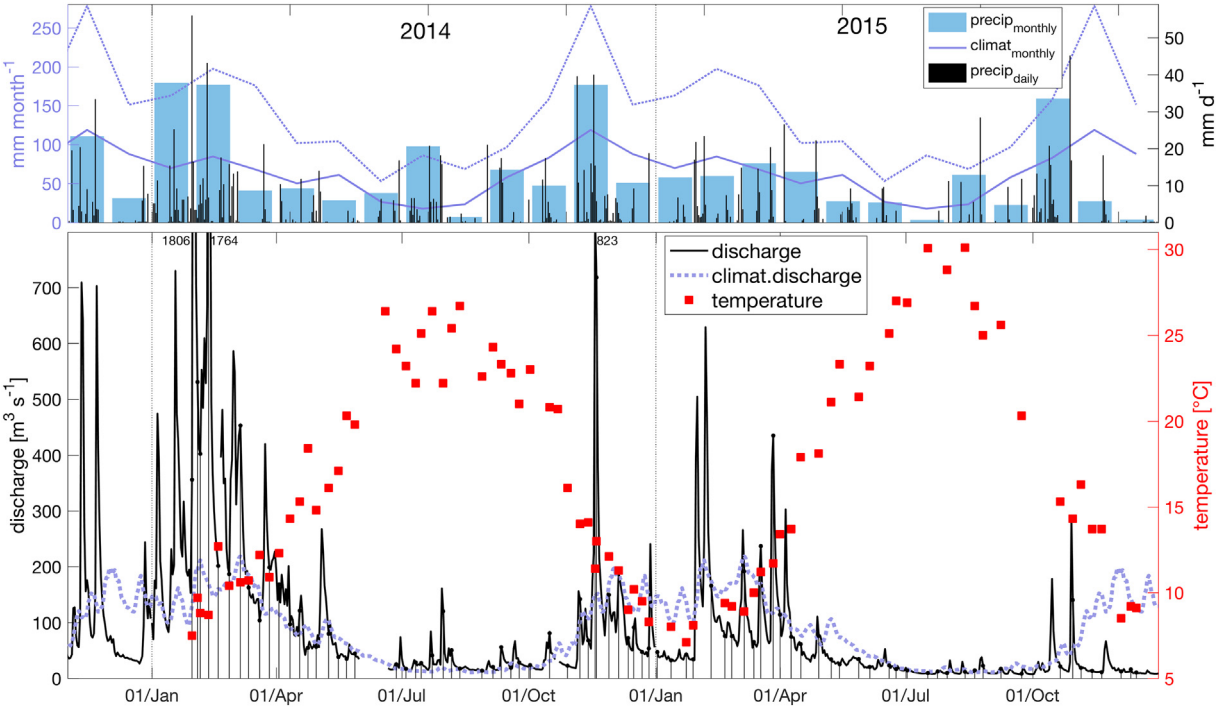

Fig. 2. Upper panel: time-series of daily (black bars) and monthly (light blue bars) precipitation, and monthly climatology (blue solid line) and 95 percentile (blue dotted line) precipitation over the Arno River drainage basin. Data from 122 meteorological stations of SIR regional service. Lower panel: time-series of daily Arno River discharge (black solid line, values exceeding 800 $m^3\ s^{-1}$ are indicated on the figure), daily climatology (dotted blue line), time of sampling (vertical grey tin lines) and temperature at the sampling (red squares). (For interpretation of the references to color in this figure legend, the reader is referred to the web version of this article.)

Table 1
List of the flood events recorded during 2014–2015 sampling period. Each event is characterized by its starting day, duration, mean daily water discharge, total DOC flux and typical return period of flood event class to which the event belongs. The return period was computed for three selected classes of flood events based on the 18-year Arno water discharge time-series: large (mean water discharge larger than 600 $m^3 s^{-1}$ and duration longer than 9 days), intermediate (one of the two criteria) and small (none of them).

Event start date	Duration (days)	Average daily discharge ($m^3 s^{-1}$)	DOC flux (10^6 g C)	Return period of flood event classes for 2002–2019 Arno discharges time-series		
				Large	Intermediate	Small
30/01/2014	18	706	3439	4.5 yr		
20/02/2014	5	376	376			2.7 months
27/02/2014	10	409	818		1.5 yr	
18/11/2014	3	640	794		1.5 yr	
30/01/2015	3	384	266			2.7 months
06/02/2015	3	455	316			2.7 months
26/03/2015	3	361	352			2.7 months

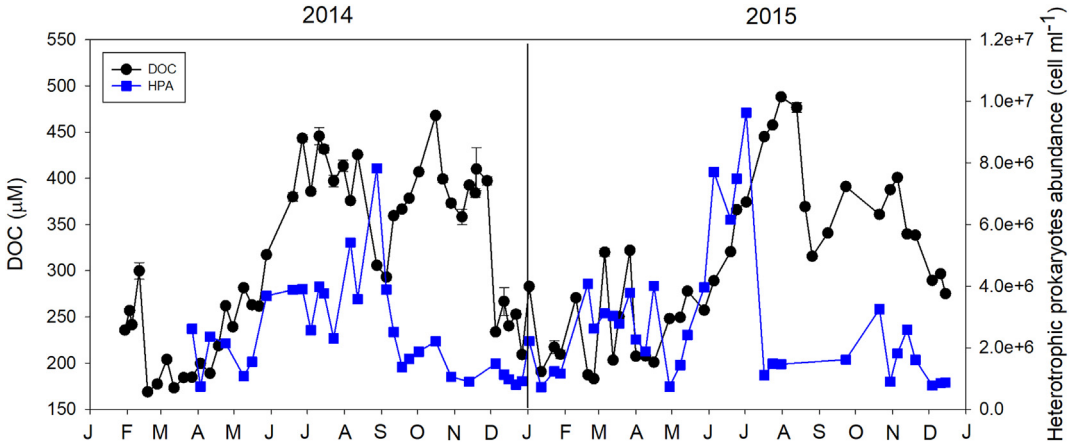

Fig. 3. Dissolved organic carbon (DOC) concentration and heterotrophic prokaryotes abundance (HPA) in 2014 and 2015. Error bars refer to the standard deviation between the three analytical replicates. The vertical line separates the two years.

3.3. DOC concentration and fluxes

DOC concentration ranged between 168 and 468 μM (average 309 ± 90 μM) in 2014, and between 183 and 488 μM (average 305 ± 84 μM) in 2015. In 2014, DOC was lower than 200 μM between January and March, excluding the flood events, when it increased up to 300 μM (Fig. 3). It steeply increased between April and June, then it ranged between 380 and 440 μM until August when a 132 μM decrease was observed followed by a 175 μM increase. The highest concentration (468 μM) was observed in mid-October. In November,

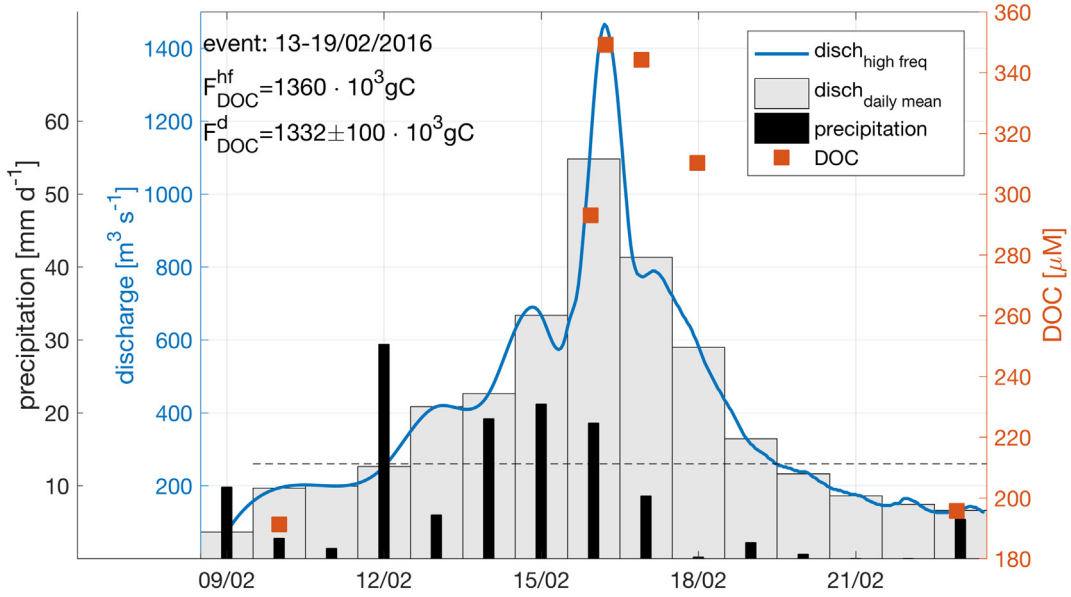

Fig. 4. High frequency (blue line) and daily (grey bars) discharge of Arno River; daily precipitation (black bars) and concentration of DOC (red dots) in February 2016. Threshold of 250 $m^3 s^{-1}$ (horizontal dashed black line) identifies the duration of the flood event (i.e., 13–19 February). Values of total DOC flux (FDOC) during the flood event are provided for the high frequency (hf) and daily (d) calculation (details of the calculations are given in the text). (For interpretation of the references to color in this figure legend, the reader is referred to the web version of this article.)

DOC was relatively high, whereas in December it decreased again to 200 μM. In 2015, between January and March, DOC showed slightly higher and more variable values than in winter 2014 (Fig. 3). It constantly increased from April to August, when it reached its annual maximum (488 μM). As observed in 2014, DOC decreased at the end of August (−173 μM), increased in September (+76 μM), it stayed relatively stable in October and decreased steadily toward the end of the year.

The weekly DOC concentration values were linearly interpolated and multiplied by the daily water discharges to obtain the riverine daily DOC flux. By averaging over the year, the estimated mean annual DOC fluxes were $12.95 \cdot 10^9$ g DOC yr^{-1} in 2014 and $5.12 \cdot 10^9$ g DOC yr^{-1} in 2015. It is noteworthy that large and intermediate flood events (Table 1), which occurs typically during winter, can significantly contribute to the annual flux of DOC to the coastal Tyrrhenian Sea. As an example, in 2014, 26% of the annual DOC flux was transported by one single large flood event (30/Jan/2014, Table 1). Due to the high variability of DOC values in winter, and the relevance of flood events for the precise calculation of the DOC fluxes, it is crucial to assess the uncertainty of the DOC flux estimation during the flood events. A flood event, occurring in winter 2016, was therefore analyzed with high frequency DOC (6, 12 and 24 h samplings) and water discharge data (15 and 30 min data, Fig. 4). The flood event started on February 13th, lasted 6 days, according to the aforementioned flood event criteria and showed a fast response to the precipitation event (Fig. 4). During the flood event, DOC concentrations remained pretty constant (i.e., coefficient of variation of 8%), with an average of 324 μM, and were different from the values before and after the flood event (mean difference of 40%). The DOC flux, computed by integrating the high frequency DOC and discharge data after linear interpolation of the DOC on discharge times, was equal to $1360 \cdot 10^3$ g for the 6-day flood event. Its uncertainty was evaluated by sub-sampling the high frequency DOC and river discharge data to the frequency regularly used in the 2014–2015 analysis. Thus, DOC flux was re-evaluated using daily discharge data and each of the high frequency DOC measurements during the flood period. The ensemble average was $1332 \cdot 10^3$ and the standard deviation, that provides the accuracy level in the case of a single DOC value available during the flood event, was $100 \cdot 10^3$ g DOC. Further, the difference of the ensemble mean with respect to the high frequency calculation was $<40 \cdot 10^3$ g DOC, allowing us to conclude that the uncertainty of DOC flux calculation, based on daily discharge and weekly sampling, can be <5%.

3.4. DOM optical properties

3.4.1. Absorption

The a_{254} ranged between 12.2 and 46.6 m^{-1} in 2014 and between 14.1 and 42.2 m^{-1} in 2015. A good correlation was found between a_{254} and DOC when the whole dataset was taken into consideration (Fig. 5a, Table 2). The a_{440} ranged between 0.2 and 2.7 m^{-1} in 2014, and between 0.6 and 2.0 m^{-1} in 2015. Similar to a_{254}, a good, although weaker ($R^2 = 0.82$), correlation was found between a_{440} and DOC (Fig. 5b; Table 2). However, when the two years were taken into consideration separately, a slightly different slope was observed for the correlation between DOC and a_{440} (Fig. 5b), but not for that between DOC and a_{254}. The $SUVA_{254}$ ranged between 5.2 and 8.1 L m^{-1} mg^{-1} in 2014 and between 6.1 and 8.2 L m^{-1} mg^{-1} in 2015.

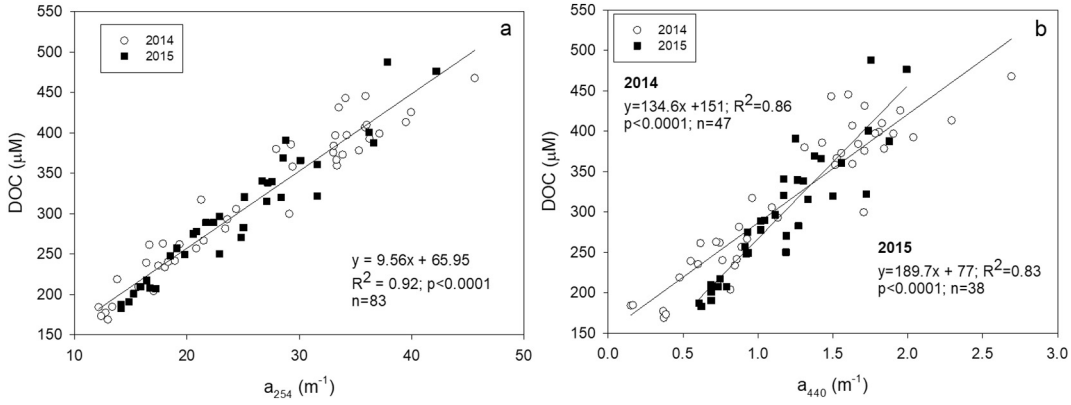

Fig. 5. Correlation between dissolved organic carbon (DOC) and the absorption coefficient at 254 nm, a_{254} (a) and the absorption coefficient at 440 nm, a_{440} (b) in the two years.

Table 2
Values of the slope (*italic*) and R^2 for the linear correlations between CDOM (absorption coefficients at 254 nm, a_{254} and at 440 nm, a_{440}), FDOM (Microbial Humic-like component $C1_{mh}$, Terrestrial Humic-like component $C2_{th}$, Terrestrial Fulvic-like component $C3_{tf}$, Protein-like component $C4_p$, and Protein + Polycyclic Aromatic Hydrocarbon-like component $C5_{pah}$) and Dissolved Organic Carbon (DOC). For all the correlations reported $p < .0001$.

	$C1_{mh}$	$C2_{th}$	$C3t_f$	$C4_p$	$C5_{pah}$	DOC	a_{254}	a_{440}
$C1_{mh}$								
$C2_{th}$	*0.272*							
	0.39							
$C3_{fh}$	*0.246*	*0.911*						
	0.35	**0.91**						
$C4_p$	*1.507*	–	–					
	0.80							
$C5_{pah}$	–	–	–	*−0.103*				
				0.21				
DOC	*124.6*	*295.1*	*292.9*	*62.61*	–			
	0.71	**0.72**	**0.64**	0.48				
a_{254}	*11.480*	*31.91*	*31.89*	*4.698*	–	*0.096*		
	0.56	**0.88**	**0.80**	0.27		**0.92**		
a_{440}	*0.597*	*1.909*	*1.917*	–	–	*0.005*	*0.059*	
	0.40	**0.84**	**0.77**			**0.80**	**0.94**	

3.4.2. Fluorescence EEMs and PARAFAC analysis

In order to identify the 5 components validated by the PARAFAC analysis, their spectra were compared with those stored in the OpenFluor database (similarity score > 0.96) (Murphy et al., 2014b) or reported in the literature (Table S2).

Component 1 (λ_{ex}: <250/305, λ_{em}: 408; Fig. 6) show excitation and emission maxima similar to the "marine" or "microbial" humic-like substances ($C1_{mh}$) (Lambert et al., 2016; Maie et al., 2014; Meng et al., 2013; Murphy et al., 2011; Parlanti et al., 2000; Yamashita et al., 2015b). Spectral characteristics of component 2 (λ_{ex}: <250/380, λ_{em}: 494; Fig. 6) are typical of the terrestrial humic-like substances ($C2_{th}$) (Lambert et al., 2016; Maie et al., 2014; Meng et al., 2013; Murphy et al., 2014a; Parlanti et al., 2000; Yamashita et al., 2015b). The emission peak of component 3 (λ_{ex}: <250/350, λ_{em}: 435; Fig. 6) is at intermediate wavelengths between $C1_{mh}$ and $C2_{th}$, suggesting its identification as terrestrial fulvic-like compound ($C3_{tf}$), in agreement with Lapierre and Del Giorgio (2014). Excitation and emission peaks of component 4 (λ_{ex}: 280, λ_{em}: 335; Fig. 6) are typical of protein-like compounds ($C4_p$) (Gonçalves-Araujo et al., 2015; Hur and Cho, 2012; Lambert et al., 2016; Meng et al., 2013; Murphy et al., 2006; Parlanti et al., 2000; Stedmon et al., 2011). The identification of component 5 (λ_{ex}: 265, λ_{em}: 330; Fig. 6) is controversial since its excitation and emission maxima are very similar to those of protein-like compounds (Ferretto et al., 2017; Maie et al., 2014; Meng et al., 2013; Yamashita et al., 2015a), but

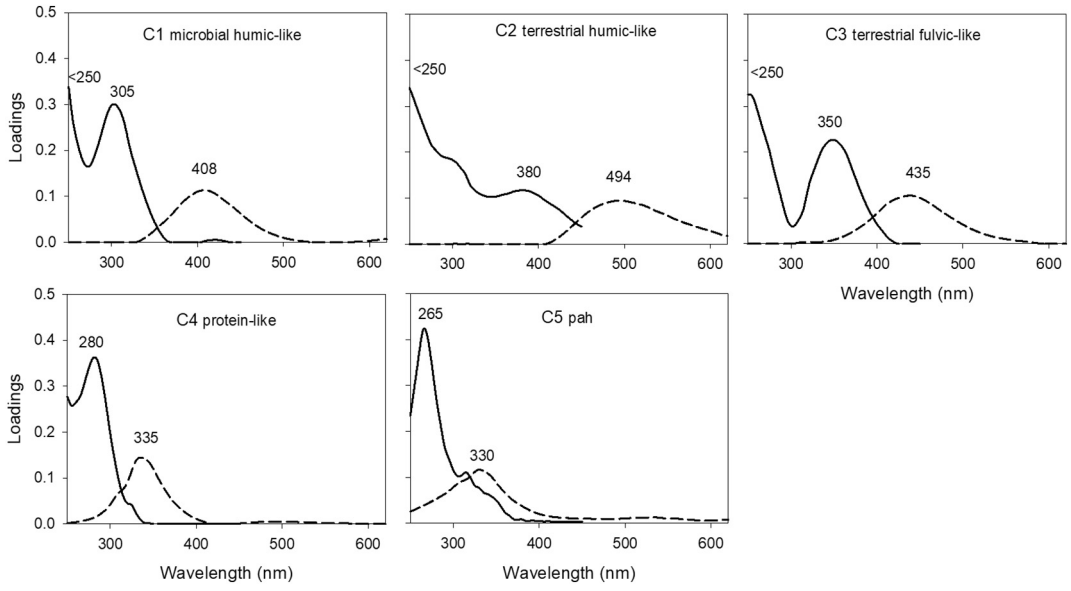

Fig. 6. Excitation (line) and emission (dashed line) spectra of the components identified by PARAFAC. The numbers indicate the peak wavelengths.

Table 3
Linear correlations between the measured parameters in winter (January–March) 2014. The slope and the R^2 of the correlations are reported. The correlations were reported only for $R^2 > 0.2$ and $p < .05$. DOC = Dissolved Organic Carbon; HPA = Heterotrophic Prokaryotes Abundance; a_{254} = absorbance at 254 nm; a_{440} = absorbance at 440 nm; $SUVA_{254}$ = Specific Ultraviolet Absorption at 254 nm; $C1_{mh}$ = Microbial Humic-like component; $C2_{th}$ = Terrestrial Humic-like component; $C3_{fh}$ = Terrestrial Fulvic-like component; $C4_p$ = Protein-like component; $C5_{pah}$ = Protein + Polycyclic Aromatic Hydrocarbon-like component.

January–March 2014	Discharge	Temperature	DOC	HPA	a_{254}	a_{440}	$SUVA_{254}$	$C1_{mh}$	$C2_{th}$	$C3_{fh}$	$C4_p$	$C5_{pah}$
Discharge												
Temperature	–											
DOC	0.07606	−20.54										
	0.72*	**0.56**										
HPA	x	x	x									
a_{254}	0.01032	−2.15	0.118	x								
	0.89**	0.41	**0.93****									
a_{440}	0.00008	–	0.009	x	0.007							
	0.87**		**0.82****		**0.94****							
$SUVA_{254}$	0.00137	–	0.013	x	0.019	0.147						
	0.85**		**0.62**		**0.81****	**0.90****						
$C1_{mh}$	0.000012	−0.032	0.016	x	0.002	0.135	0.07					
	0.65	0.47	**0.92****		**0.81****	**0.73***	0.49					
$C2_{th}$	0.000029	−0.063	0.003	x	0.001	0.326	0.19	1.93				
	0.83**	0.42	**0.93****		**0.98****	**0.94****	**0.84****	**0.82****				
$C3_{fh}$	0.000017	−0.044	0.002	x	0.002	0.199	0.12	1.27	0.63			
	0.69*	**0.51**	**0.96****		**0.92****	**0.85****	**0.70***	**0.86****	**0.96****			
$C4_p$	–	0.024	0.00009	x	0.002	–	−0.05	–	−0.25	−0.41		
		0.46	0.46		0.37		0.40		0.47	**0.51**		
$C5_{pah}$	–	–	–	x	–	–	−0.12	–	–	–	–	
							0.56					

x: no HPA data in this period.
* $p < .005$.
** $p < .0001$.

its spectral characteristics are also similar to those of synthetic and/or toxic compounds (Gonnelli et al., 2016; Kothawala et al., 2014; Li et al., 2013; Nie et al., 2016; Parlanti et al., 2000) such as naphthalene in water (Beltrán et al., 1998; Ferretto et al., 2014). As a matter of fact, naphthalene is currently used by industries (e.g. tanneries) active along the drainage basin of the Arno River. Therefore, the C5 component has been attributed to a mixture of proteins and polycyclic aromatic hydrocarbons ($C5_{pah}$).

A good linear correlation was observed between $C1_{mh}$ and $C4_p$ (Table 2) supporting that both are produced in situ, and between $C2_{th}$ and $C3_{tf}$ (Table 2), supporting that both have a terrestrial origin. In contrast, $C5_{pah}$ does not correlate with any other components. All the components, except $C5_{pah}$, showed a good correlation with DOC (Table 2).

3.5. Main drivers of DOM dynamics in the Arno River

In order to investigate the main processes affecting DOM dynamics in the Arno River, the correlations between the measured parameters were studied focusing on specific periods (Tables 3–6).

3.5.1. Winter

In 2014, between January and March, a good correlation was found between the discharge and most of the other parameters, except for temperature, $C4_p$, and $C5_{pah}$ (Table 3). In 2015, the correlation between discharge and (i) DOC, (ii) absorption (a_{254} and a_{440}), and (iii) FDOM were weaker than in 2014 (Table 4). In both years, DOC correlated well with FDOM, (all components except $C5_{pah}$, and $C4_p$ in 2015, Table 4). $C1_{mh}$ showed a good correlation with the terrestrial components ($C2_{th}$ and $C3_{fh}$) whereas no correlation was found between $C1_{mh}$ and $C4_p$ (Tables 3 and 4).

In 2014, the relationship between discharge and DOC showed a better fitting with a logarithmic curve with respect to the linear fitting (Fig. 7a). In both years, $C4_p$ decreased following a power-law function with increasing discharge (Fig. 7b).

3.5.2. Spring–summer

In both years, between April and July/August, the correlation between the discharge and the other parameters was weak (Tables 5 and 6), except for DOC, that showed a good power-law function fitting with the discharge (Fig. 8).

A very good linear correlation was found between the temperature and almost all the measured parameters, except $SUVA_{254}$. A good linear correlation was also found between the HPA and most of the parameters, with the best fitting for temperature, DOC, $C1_{mh}$ and C_p (Tables 5 and 6).

In 2015, all the correlations were weaker than in the previous year (Table 6). It is important to highlight that in 2015 the correlations with the HPA were significant only when the data collected between April and July 2nd are taken into consideration, that is the period when a continuous growth was observed.

4. Discussion

4.1. The impact of floods on DOM dynamics

The good linear correlation observed between DOC, CDOM, FDOM and discharge in the first months of both years (January to March) (Tables 3 and 4) suggests that in this period DOM dynamics is mainly controlled by the river discharge, with a significant role of the floods. The increase in DOC concentration with discharge can be mostly attributed to the increase in the water level, caused by the high discharge, and consequently to the soil leaching, as well as to the heavy rains washing out the soil. The very good correlation found between DOC and $C2_{th}$ and $C3_{tf}$ supports the terrestrial character of the DOM in this period. This is further supported by the good linear correlation between the $SUVA_{254}$ and both discharge and DOC (Tables 3 and 4) indicating that the DOC present in the river has high aromatic content and high molecular weight. The exponential decrease of C4p at increasing discharge (Fig. 7b), indicates that this autochthonous component is mainly diluted by the large water volume at the beginning of the floods. Interestingly, in 2014 when the river discharge was higher than 500 $m^3\ s^{-1}$ the best fitting between discharge and DOC, CDOM (a_{254}, a_{440}) and the terrestrial FDOM ($C2_{th}$ and $C3_{fh}$) was logarithmic, suggesting that when a large volume of water has flowed through the soil, most of its reservoir of organic matter has been leached.

Surprisingly, between January and March, DOC concentrations were higher in 2015 than in 2014 even if the discharge was similar (Fig. 7a).

Table 4
Linear correlations between the measured parameters in winter (January–March) 2015. The slope and the R^2 of the correlations are reported. The correlations were reported only for $R^2 > 0.2$ and $p < .05$. DOC = Dissolved Organic Carbon; HPA = Heterotrophic Prokaryotes Abundance; a_{254} = absorbance at 254 nm; a_{440} = absorbance at 440 nm; $SUVA_{254}$ = Specific Ultraviolet Absorption at 254 nm; $C1_{mh}$ = Microbial Humic-like component; $C2_{th}$ = Terrestrial Humic-like component; $C3_{fh}$ = Terrestrial Fulvic-like component; $C4_p$ = Protein-like component; $C5_{pah}$ = Protein + Polycyclic Aromatic Hydrocarbon-like component.

January–March 2015	Discharge	Temperature	DOC	HPA	a_{254}	a_{440}	$SUVA_{254}$	$C1_{mh}$	$C2_{th}$	$C3_{fh}$	$C4_p$	$C5_{pah}$
Discharge												
Temperature	–											
DOC	0.346 0.69*	–										
HPA	–	–	–									
a_{254}	0.045 **0.79***	–	0.119 **0.97****	–								
a_{440}	0.002 **0.83****	–	0.007 **0.96****	–	0.061 **0.99****							
$SUVA_{254}$	0.005 **0.85****	–	0.011 **0.77****	–	0.102 **0.89****	1.652 **0.88****						
$C1_{mh}$	–	−0.034 0.45	0.001 0.39	–	–	–	–					
$C2_{th}$	0.00008 0.48	–	0.003 **0.94****	–	0.023 **0.88****	0.365 **0.84****	0.185 **0.66***	0.984 **0.55***				
$C3_{fh}$	0.00006 0.40	–	0.002 **0.88****	–	0.015 **0.81****	0.241 **0.77****	0.118 **0.57**	0.712 **0.59**	0.682 **0.96****			
$C4_p$	−0.001 0.45	–	–	$-1.1 \cdot 10^{-7}$ 0.42	–	–	−0.198 **0.51**	–	–	–		
$C5_{pah}$	–	–	–	–	–	–	–	–	–	–	–	

* $p < .005$.
** $p < .0001$.

Table 5
Linear correlations between the measured parameters in spring/summer (April–July) 2014. The slope and the R^2 of the correlations are reported. The correlations were reported only for $R^2 > 0.2$ and $p < .05$. DOC = Dissolved Organic Carbon; HPA = Heterotrophic Prokaryotes Abundance; a_{254} = absorbance at 254 nm; a_{440} = absorbance at 440 nm; $SUVA_{254}$ = Specific Ultraviolet Absorption at 254 nm; $C1_{mh}$ = Microbial Humic-like component; $C2_{th}$ = Terrestrial Humic-like component; $C3_{fh}$ = Terrestrial Fulvic-like component; $C4_p$ = Protein-like component; $C5_{pah}$ = Protein + Polycyclic Aromatic Hydrocarbon-like component.

April–July 2014	Discharge	Temperature	DOC	HPA	a_{254}	a_{440}	$SUVA_{254}$	$C1_{mh}$	$C2_{th}$	$C3_{fh}$	$C4_p$	$C5_{pah}$
Discharge												
Temperature	−0.077											
	0.69**											
DOC	−1.520	18.52										
	0.52	**0.81****										
HPA	−18,600	219,695	10,254									
	0.50	**0.71***	**0.64***									
a_{254}	−0.167	1.561	0.089	$4.14 \cdot 10^{-6}$								
	0.39	**0.64***	**0.97****	0.48								
a_{440}	−0.010	0.095	0.005	$2.51 \cdot 10^{-7}$	0.055							
	0.43	**0.74****	**0.97****	**0.56**	**0.96****							
$SUVA_{254}$	–	–	0.004	–	0.054	0.864						
			0.42		**0.60***	0.49						
$C1_{mh}$	−0.008	0.106	0.006	$4.37 \cdot 10^{-7}$	0.073	1.219	–					
	0.33	**0.59***	**0.87****	**0.66***	**0.84****	**0.76****						
$C2_{th}$	−0.002	0.028	0.002	–	0.019	0.343	0.242	0.229				
	0.39	**0.58***	**0.87****		**0.93****	**0.89****	**0.68****	**0.72****				
$C3_{fh}$	−0.003	0.0314	0.002	$9.12 \cdot 10^{-8}$	0.019	0.355	0.189	0.219	0.962			
	0.46	**0.68****	**0.86****	0.41	**0.82****	**0.91****	0.40	**0.63****	**0.88****			
$C4_p$	−0.018	0.242	0.013	$1.03 \cdot 10^{-6}$	0.145	2.523	–	2.067	5.972	6.051		
	0.38	**0.66****	**0.83****	**0.79****	**0.71****	**0.70****		**0.92****	**0.56***	**0.60***		
$C5_{pah}$	0.006	−0.068	−0.003	$-2.23 \cdot 10^{-7}$	−0.028	−0.520	–	−0.412	−1.392	−1.457	−0.209	
	0.57**	**0.79****	**0.70****	**0.74****	0.48	**0.53**		**0.55***	0.46	0.48*	**0.66****	

* $p < .005$.
** $p < .0001$.

This difference can be attributed to the timing of flood events. In 2013, the Arno River had a very high average discharge (132.7 $m^3\ s^{-1}$) with several big winter floods (discharge > 500 $m^3\ s^{-1}$, Fig. S4). As a consequence, at the beginning of 2014, a large portion of the watershed had already been flushed and, when the big floods occurred in February of 2014, the DOC stock of the watershed was reduced, leading to a lower amount of DOC transported into the river. In 2014, instead, the winter average discharge (October–December) was lower than in 2013 and only one flood event occurred in November, the DOC reserve in the soil was, therefore, less depleted than in 2013 and a higher amount of DOC was leached in the river during the floods event in 2015, even if they were less intense than in 2014. The logarithmic correlation between DOC and river discharge in 2014 supports this hypothesis since when the discharge was higher than 500 $m^3\ s^{-1}$ the addition of water did not increase the DOC concentration in the river. The DOC concentrations higher in winter 2015 than 2014 may be also attributed to a higher

Table 6
Linear correlations between the measured parameters in spring/summer (April–August) 2015. The slope and the R^2 of the correlations are reported. The correlations were reported only for $R^2 > 0.2$ and $p < .05$. DOC = Dissolved Organic Carbon; HPA = Heterotrophic Prokaryotes Abundance; a_{254} = absorbance at 254 nm; a_{440} = absorbance at 440 nm; $SUVA_{254}$ = Specific Ultraviolet Absorption at 254 nm; $C1_{mh}$ = Microbial Humic-like component; $C2_{th}$ = Terrestrial Humic-like component; $C3_{fh}$ = Terrestrial Fulvic-like component; $C4_p$ = Protein-like component; $C5_{pah}$ = Protein + Polycyclic Aromatic Hydrocarbon-like component.

April–August 2015	Discharge	Temperature	DOC	HPA	a_{254}	a_{440}	$SUVA_{254}$	$C1_{mh}$	$C2_{th}$	$C3_{fh}$	$C4_p$	$C5_{pah}$
Discharge												
Temperature	−0.169											
	0.83**											
DOC	−0.47	16.253										
	0.58**	**0.86****										
HPA	−61,192	464,235	39,466									
	0.44	**0.55**	**0.64***									
a_{254}	−0.179	1.358	0.086	$1.20 \cdot 10^{-6}$								
	0.47	**0.76****	**0.97****	0.48								
a_{440}	−0.008	0.066	0.004	$5.49 \cdot 10^{-6}$	0.047							
	0.49	**0.79****	**0.96****	0.41	**0.99****							
$SUVA_{254}$	–	–	–	–	–	–						
$C1_{mh}$	−0.02	0.134	0.008	$1.50 \cdot 10^{-7}$	0.100	2.078	–					
	0.52*	**0.77****	**0.95****	**0.79****	**0.95****	**0.94****						
$C2_{th}$	−0.005	0.031	0.002	$2.75 \cdot 10^{-8}$	0.026	0.561	0.067	0.227				
	0.45	**0.66****	**0.80****	**0.56**	**0.94****	**0.96****	0.35	**0.83****				
$C3_{fh}$	−0.003	0.021	0.001	–	0.018	0.40	0.308	0.142	0.744			
	0.35	**0.50***	**0.51***		**0.68****	**0.73****	0.37	0.49*	**0.84****			
$C4_p$	−0.025	0.169	0.011	$1.83 \cdot 10^{-7}$	0.118	2.442	–	1.253	4.18	3.55		
	0.50*	**0.74****	**0.92****	**0.72****	**0.85****	**0.82****		**0.94****	**0.65****	0.31		
$C5_{pah}$	6.74 · 10–4	−0.004	–	–	–	–	–	–	–	–	−0.018	
	0.35	0.38									0.33	

* $p < .005$.
** $p < .0001$.

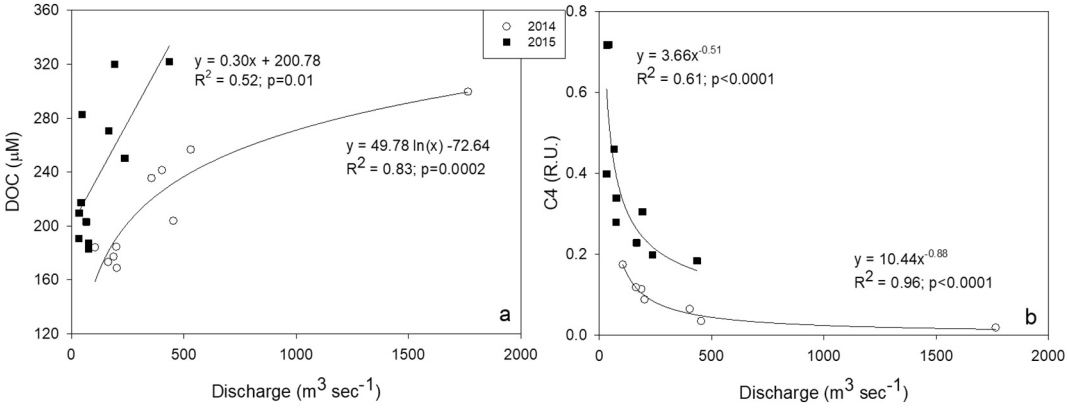

Fig. 7. Correlation between discharge and dissolved organic carbon (DOC, a) and the protein-like component, C4p (b) between January and March in the two years.

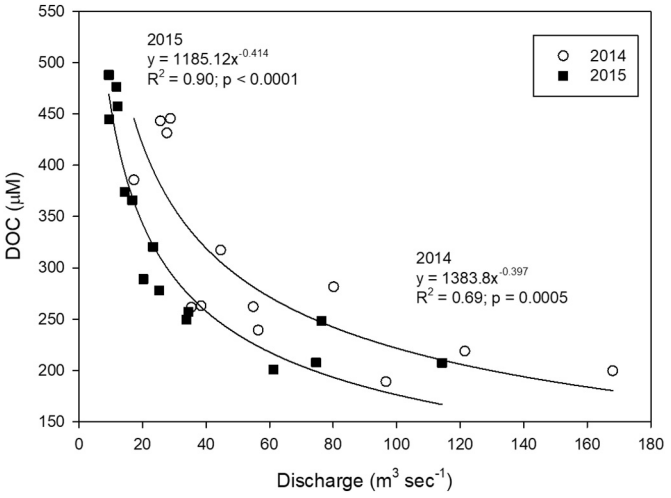

Fig. 8. Correlation between discharge and dissolved organic carbon (DOC) between April and July 2014/August 2015.

biological activity in 2015 than in 2014, releasing DOC as suggested by the good correlation between DOC and the autochthonous FDOM components ($R^2 = 0.76$ for $C1_{mh}$ and 0.91 for $C4_p$), observed in 2015, when the floods are excluded. The higher percentage of autochthonous FDOM ($C1_{mh} + C4_p$) in 2015 than in 2014 (Fig. 9) further supports this hypothesis.

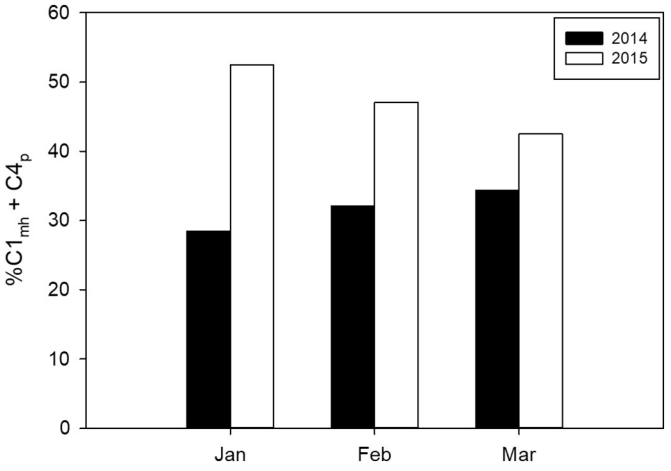

Fig. 9. Monthly average of the percentage of the autochthonous components (marine humic-like component, and protein-like component, $C1_{mh} + C4_p$) between January and March of the two years.

4.2. In situ DOM production dominates in spring and summer

The good correlation between temperature and DOC, CDOM, and FDOM, between April and July 2014 (Table 5) and between April and August 2015 (Table 6), suggests that the increase in temperature is directly and/or indirectly the main driver of DOM dynamics.

In this period, the very low discharge causes a high water residence time that, combined with the seasonal temperature increase, can stimulate biological activity (Brown et al., 2004; Gillooly, 2001; Gillooly et al., 2002), producing DOM. The in-situ DOM production is, indeed, often attributed to autotrophic activity (Carlson and Hansell, 2015; Romera-Castillo et al., 2010), enhanced during spring phytoplankton blooms. In our study, this hypothesis is supported by the predominance of the autochthonous FDOM components ($C1_{mh}$ and $C4_p$) over the terrestrial one ($C2_{th}$ and $C3_{tf}$) (Fig. 10). We also observed abundant virus-like particles (VLP) while analyzing bacteria by flow cytometry in samples from the summer (Fig. S3). Although the samples were not processed according to a virus-specific staining protocol (e.g. Brussaard et al., 2010), their occurrence may suggest viral-induced algal lysis, possibly leading to DOM release (Sheik et al., 2014). Additional measurements, including primary productivity and phytoplankton abundance, are needed in the future to confirm this hypothesis.

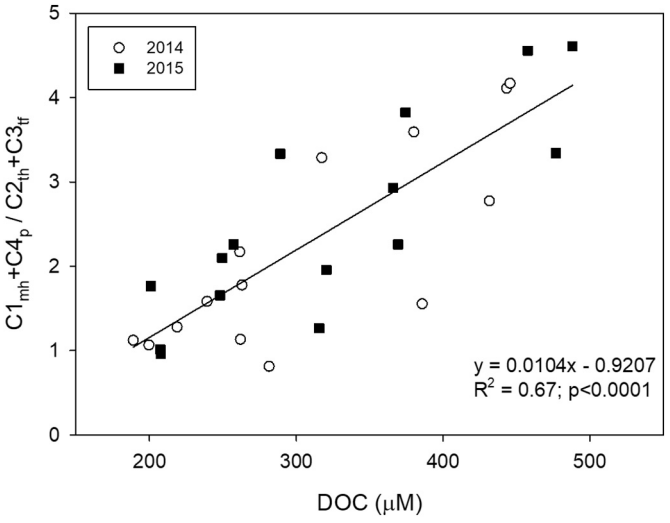

Fig. 10. Correlation between dissolved organic carbon (DOC) and the ratio between the autochthonous FDOM components (marine humic-like component $C1_{mh}$ + protein-like component $C4_p$) and the terrestrial ones (terrestrial humic-like component $C2_{th}$ + terrestrial fulvic-like component $C3_{tf}$) between April and July/August in the two years.

The increase in temperature can also favor particle dissolution with an additional release of DOM (Raymond and Spencer, 2015).

High temperature, combined with high DOM concentrations, stimulates heterotrophic activity as also shown by the good linear correlation between DOC and HPA (Tables 5 and 6). In addition, the good correlation between HPA and the autochthonous components ($C1_{mh}$ and $C4_p$), suggests that HP also contribute to FDOM release. However, we cannot exclude that the observed predominance of the protein-like components is due to photobleaching of humic-like substances, enhanced by the high spring/summer irradiation and to the high residence time of riverine water. DOM photobleaching affects the humic-like substances more than the protein-like ones, and stronger effects can be observed at longer wavelengths (Osburn et al., 2009, 2014). Photobleaching could, therefore, reduce the fluorescence of humic-like components making the protein-like substances dominant.

DOC dynamic is different in the spring/summer of the two years. In 2014, DOC increases between April and the end of June, then it remained at about 400 μM until the end of August. In 2015, instead, it constantly increases between April and August (Fig. 3). Interestingly, this trend corresponds to the trend in temperature (Fig. 2). The lower and more variable temperature in 2014 than in 2015 was probably caused by the anomalous rainier weather in summer 2014 (Ratna et al., 2017). This good correspondence between DOC and temperature trends suggests that weather conditions can be a crucial factor affecting DOM dynamics in riverine ecosystems.

4.3. Impact of the Arno River on the Med Sea C cycle

The 2 year-data reported in this study, given their representativeness of the river discharge in the last 17 years, provide a robust estimate of the Arno River C fluxes to the Med Sea and its range of variability. By using the average DOC concentration in the 2 years and the average discharge of the river in the last 17 years, a flux of $9.6 \cdot 10^9$ g DOC yr^{-1} (range $12.95 \cdot 10^9$–$5.12 \cdot 10^9$ g DOC yr^{-1}) was estimated. The 80% of this flux was generally delivered during autumn/winter (i.e., mean daily fluxes during winter and summer were $38 \cdot 10^6$ and $11 \cdot 10^6$ g DOC d^{-1}, respectively), with significant amounts ascribed to flood events (up to 26% in 2014). This is true also in "dry" years, such as 2015, when the DOC maximum annual flux was delivered during small flood events.

Our data also show that DOC flux in 2014 and 2015 represented up to 7% of the total estimated DOC fluxes for the western basin of the Med Sea even if Arno River water discharge is ~2% of the total river discharges (Santinelli, 2015). In addition, the Arno River DOC yield (DOC flux/basin area: 0.76–2.38 g C m^{-2} yr^{-1}) reached values twice the average DOC yield of all the rivers discharging into the Med Sea (1.08 g C m^{-2} yr^{-1}, Santinelli, 2015) and it is surprisingly close to the average DOC yield calculated for the 30 major world rivers (2.3 g C m^{-2} yr^{-1}) (Raymond and Spencer, 2015). These calculations stress the crucial role of small river in the carbon budget of the Med Sea. Unfortunately, for most of the rivers discharging into the Med Sea, no precise estimate of DOC fluxes are reported, since the calculation is usually done by taking into consideration the average discharge and the DOC concentration measured sporadically (e.g. Santinelli, 2015).

Our data point to a clear seasonal cycle of DOM, with DOC values ranging between 170 and 490 μM within 1 year. Due to the high variability of DOC concentration, the use of only 1 or few values of concentration can therefore lead to significant over or underestimations of DOC fluxes.

Water quantity and quality discharges can be simulated by hydrological models (such as the SWAT model, Arnold et al., 2012), that allow for a quantitative assessment of the water discharges and DOC and nutrients transport and possible changes due to predicted climate changes (e.g. Bhatta et al., 2019) and alternative management scenario (e.g. Malagó et al., 2019). Such models, that require a huge amount of data on the specific drainage basin domain (e.g., topographic, land use and management, and meteorological data), should be calibrated and validated. Thus, our results, by providing a rich dataset on water quantity and quality and by quantifying the importance of the hydrological regime on the DOC transport, represent an important step toward a quantitative modeling of the Arno River.

4.4. Implications for future changes

Numerical models predict that, by 2050, flood events will occur at least twice as frequently across 40% of the globe (Arnell and Gosling, 2016). For the Arno River, Alfieri et al. (2015) showed (i) a possible reduction of the average discharge and (ii) an increase of the frequency of flood events by the end of the 21st century. By reflecting our results on the importance of flood-related DOC transport against the aforementioned predicted effects of climate change, it is reasonable to hypothesize that some different scenarios, with considerable impacts on coastal ecosystems, are expected.

The expected reduction of the average discharge, and consequently the higher residence time of the water, together with higher irradiation in spring and summer can enhance the photodegradation processes, increasing the production of CO_2 and other hazardous volatile compounds such as reactive oxygen species. In addition, photochemical processes can change the biological lability of DOM (Bowen et al., 2020; Mopper et al., 2015) and can affect CDOM, reducing its role in screening the organisms from harmful UV radiations in coastal ecosystems.

The increase in flood events frequency will increase the pulsed input of unprocessed terrestrial DOM in the coastal area, as suggested by the 'pulse shunt concept' (Raymond et al., 2016). In the Arno River, during large floods (i.e. discharge >600 m^3 s^{-1}, Table 1) the water takes <3 h to flow from the sampling station to the coastal area; during minor floods (between 250 and 600 m^3 sec^{-1}) the water takes <6 h to flow from the sampling station to the sea suggesting that the large amount of DOM reaches the coastal area without being processed in the lower part of the river. This input mainly occur in winter, when primary production is at its minimum; riverine DOM may therefore represents the main source of energy to the coastal ecosystem. The DOM and nutrients coming from the river can stimulate the heterotrophic prokaryotes activity increasing the amount of CO_2 released by respiration. In addition, the large amount of DOM reaching coastal area in short time could reduce the amount and quality of photosynthetically active radiation to coastal autotrophic organisms (Stedmon and Nelson, 2015; Urtizberea et al., 2013), reducing C sequestration through photosynthesis.

Floods can also have a strong impact on the terrestrial ecosystem, impoverishing the DOM content of the alluvial soil (Saint-Laurent et al., 2016).

5. Conclusions and future directions

The DOM dynamics and transport are quantified for the Arno River, a typical example of Mediterranean small rivers with medium-high human impact, which are poorly investigated.

Even if this study only covers 2 years, they are representative of the hydrology of Arno River in the last 17 years and allows to support that DOM in the Arno River exhibited a clear annual cycle, calling for a general feature where DOM is dominated by terrestrial compounds in winter, when flood events markedly affect its dynamics, and by autochthonous compounds in spring and summer.

Our results point to the need for high time-resolved sampling to obtain accurate estimates of carbon fluxes derived from rivers. The good correlation between DOC and CDOM suggests that satellite estimates of CDOM could help in obtaining such high time-resolved data.

Regardless of its relatively low water discharge, the Arno River accounted for up to 7% of the total DOC flux into the western Med Sea in 2014 and 2015, highlighting its relevant contribution to the C budget of the Med Sea, and calling for a better re-evaluation of small rivers contribution to the global C cycle. The results showed that 80% of the DOC

flux was delivered during the autumn/winter season and that single winter flood events corresponded to DOC maximum annual flux in both years, in spite of the marked differences in average discharge and flood intensity, highlighting the crucial role that flood events play on DOM input into coastal areas and consequently in the C cycle in the Med Sea.

Our study provides a rich dataset on water quantity and quality and quantify the importance of the hydrological regime on the DOC transport, representing an important step toward a quantitative modeling of the Arno River.

Declaration of competing interests

The authors declare that they have no known competing financial interests or personal relationships that could have appeared to influence the work reported in this paper.

CRediT authorship contribution statement

Retelletti Brogi Simona: Conceptualization, Investigation, Formal analysis, Data curation, Visualization, Writing - original draft, Writing - review & editing. **Balestra Cecilia:** Formal analysis, Investigation. **Casotti Raffaella:** Resources, Formal analysis, Writing - original draft. **Cossarini Gianpiero:** Formal analysis, Visualization, Writing - review & editing. **Galletti Yuri:** Investigation, Writing - review & editing. **Gonnelli Margherita:** Conceptualization, Investigation, Writing - original draft. **Vestri Stefano:** Formal analysis, Investigation. **Santinelli Chiara:** Conceptualization, Investigation, Resources, Supervision, Funding acquisition, Writing - original draft, Writing - review & editing.

Acknowledgments

This research was supported by the PERSEUS project, funded by the European Commission under Seventh Framework Program Theme “Oceans of Tomorrow” OCEAN.2011-3, Grant Agreement No. 287600 and the Italian Flagship project RITMARE funded by the Italian Ministry of Research and University. We thank Lorenzo Mercadante and Erika Marchetti for their support in the sampling.

Appendix A. Supplementary data

Supplementary data to this article can be found online at https://doi.org/10.1016/j.scitotenv.2020.139212.

References

Aiken, G.R., Hsu-Kim, H., Ryan, J.N., 2011. Influence of dissolved organic matter on the environmental fate of metals, nanoparticles, and colloids. Environ. Sci. Technol. https://doi.org/10.1021/es103992s.

Alfieri, L., Burek, P., Feyen, L., Forzieri, G., 2015. Global warming increases the frequency of river floods in Europe. Hydrol. Earth Syst. Sci. https://doi.org/10.5194/hess-19-2247-2015.

van Apeldoorn, D., Bouwman, L., 2012. SES Land-Based Runoff and Nutrient Load Data (1980–2020). Deliverable Nr. 4.6. Policy-Oriented Marine Environmental Research in the Southern EUropean Seas (PERSEUS). Available at. http://www.perseus-net.eu/assets/media/PDF/deliverables/3321.6_Final.pdf.

Arnell, N.W., Gosling, S.N., 2016. The impacts of climate change on river flood risk at the global scale. Clim. Chang. 134, 387–401. https://doi.org/10.1016/S0003-2670(98)00420-65.

Arnold, J.G., Moriasi, D.N., Gassman, P.W., Abbaspour, K.C., White, M.J., Srinivasan, R., Santhi, C., Harmel, R.D., Van Griensven, A., Van Liew, M.W., Kannan, N., Jha, M.K., 2012. SWAT: model use, calibration, and validation. Trans. ASABE https://doi.org/10.13031/2013.42259.

Asmala, E., Bowers, D.G.D.G., Autio, R., Kaartokallio, H., Thomas, D.N., 2014. Qualitative changes of riverine dissolved organic matter at low salinities due to flocculation. J. Geophys. Res. Biogeosci. 119, 1919–1933. https://doi.org/10.1002/2014JG002722.

Balestra, C., Alonso-Sáez, L., Gasol, J.M., Casotti, R., 2011. Group-specific effects on coastal bacterioplankton of polyunsaturated aldehydes produced by diatoms. Aquat. Microb. Ecol. 63, 123–131. https://doi.org/10.3354/ame01486.

Battin, T.J., Kaplan, L.A., Findlay, S., Hopkinson, C.S., Marti, E., Packman, A.I., Newbold, J.D., Sabater, F., 2008. Biophysical controls on organic carbon fluxes in fluvial networks. Nat. Geosci. 1, 95–100. https://doi.org/10.1038/ngeo101.

Beltrán, J.L., Ferrer, R., Guiteras, J., 1998. Multivariate calibration of polycyclic aromatic hydrocarbon mixtures from excitation–emission fluorescence spectra. Anal. Chim. Acta 373, 311–319. https://doi.org/10.1016/S0003-2670(98)00420-6.

Berto, D., Giani, M., Savelli, F., 2010. Winter to spring variations of chromophoric dissolved organic matter in a temperate estuary (Po River, northern Adriatic Sea). Mar. Environ. Res. 70, 73–81. https://doi.org/10.1016/j.marenvres.2010.03.005.

Bhatta, B., Shrestha, S., Shrestha, P.K., Talchabhadel, R., 2019. Evaluation and application of a SWAT model to assess the climate change impact on the hydrology of the Himalayan River basin. Catena https://doi.org/10.1016/j.catena.2019.104082.

Bianchi, T.S., Garcia-Tigreros, F., Yvon-Lewis, S.A., Shields, M., Mills, H.J., Butman, D., Osburn, C., Raymond, P., Shank, G.C., DiMarco, S.F., Walker, N., Reese, B.K., Mullins-Perry, R., Quigg, A., Aiken, G.R., Grossman, E.L., 2013. Enhanced transfer of terrestrially derived carbon to the atmosphere in a flooding event. Geophys. Res. Lett. 40, 116–122. https://doi.org/10.1029/2012GL054145.

Bouvier, T., Del Giorgio, P.A., Gasol, J.M., 2007. A comparative study of the cytometric characteristics of high and low nucleic-acid bacterioplankton cells from different aquatic ecosystems. Environ. Microbiol. https://doi.org/10.1111/j.1462-2920.2007.01321.x.

Bowen, J.C., Kaplan, L.A., Cory, R.M., 2020. Photodegradation disproportionately impacts biodegradation of semi-labile DOM in streams. Limnol. Oceanogr. https://doi.org/10.1002/lno.11244.

Brown, J.H., Gillooly, J.F., Allen, A.P., Savage, V.M., West, G.B., 2004. Toward a metabolic theory of ecology. Ecology 85, 1771–1789. https://doi.org/10.1890/03-9000.

Brussaard, C.P.D., Payet, J.P., Winter, C., Weinbauer, M.G., 2010. Quantification of aquatic viruses by flow cytometry. Manual of Aquatic Viral Ecology. https://doi.org/10.4319/mave.2010.978-0-9845591-0-7.102.

Butturini, A., Guarch, A., Romaní, A.M., Freixa, A., Amalfitano, S., Fazi, S., Ejarque, E., 2016. Hydrological conditions control in situ DOM retention and release along a Mediterranean river. Water Res. 99, 33–45. https://doi.org/10.1016/j.watres.2016.04.036.

Caporali, E., Rinaldi, M., Casagli, N., 2005. The Arno River floods. G. di Geol. Appl. https://doi.org/10.1474/GGA.2005-01.0-18.0018.

Carlson, R.E., Fritsch, F.N., 1989. An algorithm for monotone piecewise bicubic interpolation. SIAM J. Numer. Anal. 26, 230–238. https://doi.org/10.1137/0726013.

Carlson, C.A., Hansell, D.A., 2015. DOM sources, sinks, reactivty, and budgets. Biogeochemistry of Marine Dissolved Organic Matter, pp. 65–126. https://doi.org/10.1016/B978-0-12-405940-5.00003-0.

Cauwet, G., 2002. DOM in the coastal zone. Biogeochem. Mar. Dissolved Org. Matter, 579–609 https://doi.org/10.1016/B978-012323841-2/50014-2.

Cortecci, G., Boschetti, T., Dinelli, E., Cidu, R., Podda, F., Doveri, M., 2009. Geochemistry of trace elements in surface waters of the Arno River basin, northern Tuscany, Italy. Appl. Geochem. https://doi.org/10.1016/j.apgeochem.2009.03.002.

Crump, B.C., Peterson, B.J., Raymond, P.A., Amon, R.M.W., Rinehart, A., McClelland, J.W., Holmes, R.M., 2009. Circumpolar synchrony in big river bacterioplankton. Proc. Natl. Acad. Sci. U. S. A. https://doi.org/10.1073/pnas.0906149106.

Dai, M., Yin, Z., Meng, F., Liu, Q., Cai, W.J., 2012. Spatial distribution of riverine DOC inputs to the ocean: an updated global synthesis. Curr. Opin. Environ. Sustain. https://doi.org/10.1016/j.cosust.2012.03.003.

Del Giorgio, P.A., Pace, M.L., 2008. Relative independence of organic carbon transport and processing in a large temperate river: the Hudson River as both pipe and reactor. Limnol. Oceanogr. 53, 185–197. https://doi.org/10.4319/lo.2008.53.1.0185.

Dinelli, E., Cortecci, G., Lucchini, F., Zantedeschi, E., 2005. Sources of major and trace elements in the stream sediments of the Arno River catchment (northern Tuscany, Italy). Geochem. J. https://doi.org/10.2343/geochemj.39.531.

Elliott, S., Lead, J.R., Baker, A., 2006. Characterisation of the fluorescence from freshwater, planktonic bacteria. Water Res. 40, 2075–2083. https://doi.org/10.1016/j.watres.2006.03.017.

EU Statistics, 2015. LUCAS — land use and cover area frame survey database [WWW document]. URL. https://ec.europa.eu/eurostat/web/lucas/data/database.

Fasching, C., Behounek, B., Singer, G.A., Battin, T.J., 2014. Microbial degradation of terrigenous dissolved organic matter and potential consequences for carbon cycling in brown-water streams. Sci. Rep. 4, 4981. https://doi.org/10.1038/srep04981.

Fellman, J.B., Hood, E., Spencer, R.G.M., 2010. Fluorescence spectroscopy opens new windows into dissolved organic matter dynamics in freshwater ecosystems: a review. Limnol. Oceanogr. 55, 2452–2462. https://doi.org/10.4319/lo.2010.55.6.2452.

Ferretto, N., Tedetti, M., Guigue, C., Mounier, S., Redon, R., Goutx, M., 2014. Identification and quantification of known polycyclic aromatic hydrocarbons and pesticides in complex mixtures using fluorescence excitation-emission matrices and parallel factor analysis. Chemosphere 107, 344–353. https://doi.org/10.1016/j.chemosphere.2013.12.087.

Ferretto, N., Tedetti, M., Guigue, C., Mounier, S., Raimbault, P., Goutx, M., 2017. Spatio-temporal variability of fluorescent dissolved organic matter in the Rhône River delta and the Fos-Marseille marine area (NW Mediterranean Sea, France). Environ. Sci. Pollut. Res. 24, 4973–4989. https://doi.org/10.1007/s11356-016-8255-z.

Findlay, S., 2010. Stream microbial ecology. J. North Am. Benthol. Soc. 29, 170–181. https://doi.org/10.1899/09-023.1.

Fisher, S.G., Sponseller, R.A., Heffernan, J.B., 2004. Horizons in stream biogeochemistry: flowpaths to progress. Ecology https://doi.org/10.1890/03-0244.

Gillooly, J.F., 2001. Effects of size and temperature on metabolic rate. Science 293, 2248–2251. https://doi.org/10.1126/science.1061967.

Gillooly, J.F., Charnov, E.L., West, G.B., Savage, V.M., Brown, J.H., 2002. Effects of size and temperature on developmental time. Nature 417, 70–73. https://doi.org/10.1038/417070a.

Gómez-Gutiérrez, A.I., Jover, E., Bodineau, L., Albaigés, J., Bayona, J.M., 2006. Organic contaminant loads into the Western Mediterranean Sea: estimate of Ebro River inputs. Chemosphere 65, 224–236. https://doi.org/10.1016/j.chemosphere.2006.02.058.

Gonçalves-Araujo, R., Stedmon, C.A., Heim, B., Dubinenkov, I., Kraberg, A., Moiseev, D., Bracher, A., 2015. From fresh to marine waters: characterization and fate of dissolved

organic matter in the Lena River Delta region, Siberia. Front. Mar. Sci. 2, 108. https://doi.org/10.3389/fmars.2015.00108.
Gonnelli, M., Vestri, S., Santinelli, C., 2013. Chromophoric dissolved organic matter and microbial enzymatic activity. A biophysical approach to understand the marine carbon cycle. Biophys. Chem. 182, 79–85. https://doi.org/10.1016/j.bpc.2013.06.016.
Gonnelli, M., Galletti, Y., Marchetti, E., Mercadante, L., Retelletti Brogi, S., Ribotti, A., Sorgente, R., Vestri, S., Santinelli, C., 2016. Dissolved organic matter dynamics in surface waters affected by oil spill pollution: results from the serious game exercise. Deep-Sea Res. II 133, 88–99. https://doi.org/10.1016/j.dsr2.2016.05.027.
Griffith, D.R., Raymond, P.A., 2011. Multiple-source heterotrophy fueled by aged organic carbon in an urbanized estuary. Mar. Chem. 124, 14–22. https://doi.org/10.1016/j.marchem.2010.11.003.
Hansell, D.A., 2005. Dissolved organic carbon reference material program. EOS Trans. Am. Geophys. Union 86, 318. https://doi.org/10.1029/2005EO350003.
Hitchcock, J.N., Mitrovic, S.M., 2015. After the flood: changing dissolved organic carbon bioavailability and bacterial growth following inflows to estuaries. Biogeochemistry 124, 219–233. https://doi.org/10.1007/s10533-015-0094-3.
Hur, J., Cho, J., 2012. Prediction of BOD, COD, and total nitrogen concentrations in a typical urban river using a fluorescence excitation-emission matrix with PARAFAC and UV absorption indices. Sensors 12, 972–986. https://doi.org/10.3390/s120100972.
Jaffé, R., McKnight, D., Maie, N., Cory, R., McDowell, W.H., Campbell, J.L., 2008. Spatial and temporal variations in DOM composition in ecosystems: the importance of long-term monitoring of optical properties. J. Geophys. Res. Biogeosci. https://doi.org/10.1029/2008JG000683.
Kaiser, E., Arscott, D.B., Tockner, K., Sulzberger, B., 2004. Sources and distribution of organic carbon and nitrogen in the Tagliamento River, Italy. Aquat. Sci. - Res. Across Boundaries 66, 103–116. https://doi.org/10.1007/s00027-003-0683-4.
Kothawala, D.N., Stedmon, C.A., Müller, R.A., Weyhenmeyer, G.A., Köhler, S.J., Tranvik, L.J., 2014. Controls of dissolved organic matter quality: evidence from a large-scale boreal lake survey. Glob. Chang. Biol. 20, 1101–1114. https://doi.org/10.1111/gcb.12488.
Lakowicz, J.R., 2006. Principles of Fluorescence Spectroscopy. https://doi.org/10.1007/978-0-387-46312-4.
Lambert, T., Teodoru, C.R., Nyoni, F.C., Bouillon, S., Darchambeau, F.F., Massicotte, P., Borges, A.V., 2016. Along-stream transport and transformation of dissolved organic matter in a large tropical river. Biogeosciences 13, 2727–2741. https://doi.org/10.5194/bg-13-2727-2016.
Lapierre, J.F., Del Giorgio, P.A., 2014. Partial coupling and differential regulation of biologically and photochemically labile dissolved organic carbon across boreal aquatic networks. Biogeosciences 11, 5969–5985. https://doi.org/10.5194/bg-11-5969-2014.
Lawaetz, A.J., Stedmon, C.A., 2009. Fluorescence intensity calibration using the Raman scatter peak of water. Appl. Spectrosc. 63, 936–940. https://doi.org/10.1366/000370209788964548.
Li, W.T., Xu, Z.X., Li, A.M., Wu, W., Zhou, Q., Wang, J.N., 2013. HPLC/HPSEC-FLD with multi-excitation/emission scan for EEM interpretation and dissolved organic matter analysis. Water Res. 47, 1246–1256. https://doi.org/10.1016/j.watres.2012.11.040.
Louis, Y., Garnier, C., Lenoble, V., Mounier, S., Cukrov, N., Omanović, D., Pižeta, I., 2009. Kinetic and equilibrium studies of copper-dissolved organic matter complexation in water column of the stratified Krka River estuary (Croatia). Mar. Chem. 114, 110–119. https://doi.org/10.1016/j.marchem.2009.04.006.
Ludwig, W., Probst, J.L., 1996. Predicting the oceanic input of organic carbon by continental erosion. Glob. Biogeochem. Cycles https://doi.org/10.1029/95GB02925.
Maie, N., Sekiguchi, S., Watanabe, A., Tsutsuki, K., Yamashita, Y., Melling, L., Cawley, K.M., Shima, E., Jaffé, R., 2014. Dissolved organic matter dynamics in the oligo/meso-haline zone of wetland-influenced coastal rivers. J. Sea Res. 91, 58–69. https://doi.org/10.1016/j.seares.2014.02.016.
Malagó, A., Bouraoui, F., Pastori, M., Gelati, E., 2019. Modelling nitrate reduction strategies from diffuse sources in the Po River basin. Water (Switzerland) https://doi.org/10.3390/w11051030.
Meng, F., Huang, G., Yang, X., Li, Z., Li, J., Cao, J., Wang, Z., Sun, L., 2013. Identifying the sources and fate of anthropogenically impacted dissolved organic matter (DOM) in urbanized rivers. Water Res. 47, 5027–5039. https://doi.org/10.1016/j.watres.2013.05.043.
Miller, C., Gordon, K.G., Kieber, R.J., Willey, J.D., Seaton, P.J., 2009. Chemical characteristics of chromophoric dissolved organic matter in rainwater. Atmos. Environ. 43, 2497–2502. https://doi.org/10.1016/j.atmosenv.2009.01.056.
Mladenov, N., Huntsman-Mapila, P., Wolski, P., Masamba, W.R.L., McKnight, D.M., 2008. Dissolved organic matter accumulation, reactivity, and redox state in ground water of a recharge wetland. Wetlands https://doi.org/10.1672/07-140.1.
Mopper, K., Kieber, D.J., Stubbins, A., 2015. Marine photochemistry of organic matter. Biogeochemistry of Marine Dissolved Organic Matter. https://doi.org/10.1016/b978-0-12-405940-5.00008-x.
Murphy, K.R., Ruiz, G.M., Dunsmuir, W.T.M., Waite, T.D., 2006. Optimized parameters for fluorescence-based verification of ballast water exchange by ships. Environ. Sci. Technol. 40, 2357–2362. https://doi.org/10.1021/es0519381.
Murphy, K.R., Hambly, A., Singh, S., Henderson, R.K., Baker, A., Stuetz, R., Khan, S.J., 2011. Organic matter fluorescence in municipal water recycling schemes: toward a unified PARAFAC model. Environ. Sci. Technol. 45, 2909–2916. https://doi.org/10.1021/es103015e.
Murphy, K.R., Stedmon, C.A., Graeber, D., Bro, R., 2013. Fluorescence spectroscopy and multi-way techniques. PARAFAC. Anal. Methods 5, 6557. https://doi.org/10.1039/c3ay41160e.
Murphy, K.R., Bro, R., Stedmon, C.A., 2014a. Chemometric analysis of organic matter fluorescence. Aquatic Organic Matter Fluorescence, pp. 339–375.
Murphy, K.R., Stedmon, C.A., Wenig, P., Bro, R., 2014b. OpenFluor — an online spectral library of auto-fluorescence by organic compounds in the environment. Anal. Methods 6, 658–661. https://doi.org/10.1039/C3AY41935E.
Nebbioso, A., Piccolo, A., 2013. Molecular characterization of dissolved organic matter (DOM): a critical review. Anal. Bioanal. Chem. https://doi.org/10.1007/s00216-012-6363-2.
Nie, Z., Wu, X., Huang, H., Fang, X., Xu, C., Wu, J., Liang, X., Shi, J., 2016. Tracking fluorescent dissolved organic matter in multistage rivers using EEM-PARAFAC analysis: implications of the secondary tributary remediation for watershed management. Environ. Sci. Pollut. Res. 23, 8756–8769. https://doi.org/10.1007/s11356-016-6110-x.
Omanović, D., Santinelli, C., Marcinek, S., Gonnelli, M., 2019. ASFit — an all-inclusive tool for analysis of UV–Vis spectra of colored dissolved organic matter (CDOM). Comput. Geosci. https://doi.org/10.1016/j.cageo.2019.104334.
Opsahl, S., Benner, R., 1998. Photochemical reactivity of dissolved lignin in river and ocean waters. Limnol. Oceanogr. 43, 1297–1304. https://doi.org/10.4319/lo.1998.43.6.1297.
Osburn, C.L., Retamal, L., Vincent, W.F., 2009. Photoreactivity of chromophoric dissolved organic matter transported by the Mackenzie River to the Beaufort Sea. Mar. Chem. 115, 10–20. https://doi.org/10.1016/j.marchem.2009.05.003.
Osburn, C.L., Del Vecchio, R., Boyd, T.J., 2014. Physicochemical effects on dissolved organic matter fluorescence in natural waters. Aquatic Organic Matter Fluorescence. https://doi.org/10.1017/cbo9781139045452.012.
Panagiotopoulos, C., Sempéré, R., Para, J., Raimbault, P., Rabouille, C., Charrière, B., 2012. The composition and flux of particulate and dissolved carbohydrates from the Rhone River into the Mediterranean Sea. Biogeosciences 9, 1827–1844. https://doi.org/10.5194/bg-9-1827-2012.
Para, J., Coble, P.G., Charrière, B., Tedetti, M., Fontana, C., Sempéré, R., Charrì Ere, B., Tedetti, M., Fontana, C., Sempéré, R., 2010. Fluorescence and absorption properties of chromophoric dissolved organic matter (CDOM) in coastal surface waters of the northwestern Mediterranean Sea, influence of the Rhône River. Biogeosciences 7, 4083–4103. https://doi.org/10.5194/bg-7-4083-2010.
Parlanti, E., Worz, K., Geoffroy, L., Lamotte, M., Wörz, K., Geoffroy, L., Lamotte, M., 2000. Dissolved organic matter fluorescence spectroscopy as a tool to estimate biological activity in a coastal zone submitted to anthropogenic inputs. Org. Geochem. 31, 1765–1781. https://doi.org/10.1016/S0146-6380(00)00124-8.
Pettine, M., Patrolecco, L., Camusso, M., Crescenzio, S., 1998. Transport of carbon and nitrogen to the northern Adriatic Sea by the Po River. Estuar. Coast. Shelf Sci. 46, 127–142. https://doi.org/10.1006/ecss.1997.0303.
Ratna, S.B., Ratnam, J.V., Behera, S.K., Cherchi, A., Wang, W., Yamagata, T., 2017. The unusual wet summer (July) of 2014 in southern Europe. Atmos. Res. https://doi.org/10.1016/j.atmosres.2017.01.017.
Raymond, P.A., Spencer, R.G.M., 2015. Riverine DOM. Biogeochemistry of Marine Dissolved Organic Matter, Second edition, pp. 509–533. https://doi.org/10.1016/B978-0-12-405940-5.00011-X.
Raymond, P.A., Saiers, J.E., Sobczak, W.V., 2016. Hydrological and biogeochemical controls on watershed dissolved organic matter transport: pulse-shunt concept. Ecology https://doi.org/10.1890/14-1684.1.
Reichstein, M., Bahn, M., Ciais, P., Frank, D., Mahecha, M.D., Seneviratne, S.I., Zscheischler, J., Beer, C., Buchmann, N., Frank, D.C., Papale, D., Rammig, A., Smith, P., Thonicke, K., Van Der Velde, M., Vicca, S., Walz, A., Wattenbach, M., 2013. Climate extremes and the carbon cycle. Nature https://doi.org/10.1038/nature12350.
Retelletti Brogi, S., Gonnelli, M., Vestri, S., Santinelli, C., 2015. Biophysical processes affecting DOM dynamics at the Arno River mouth (Tyrrhenian Sea). Biophys. Chem. 197, 1–9.
Romera-Castillo, C., Sarmento, H., Alvarez-Salgado, X. a, Gasol, J.M., Marrase, C., Álvarez-Salgado, X.A., Castillo, C.R., Sarmento, H., Álvarez-Salgado, X.A., Gasol, J.M., Marraséa, C., 2010. Production of chromophoric dissolved organic matter by marine phytoplankton. Limnol. Oceanogr. 55, 446–454. https://doi.org/10.4319/lo.2010.55.1.0446.
Saint-Laurent, D., Paradis, R., Drouin, A., Gervais-Beaulac, V., 2016. Impacts of floods on organic carbon concentrations in alluvial soils along hydrological gradients using a digital elevation model (DEM). Water https://doi.org/10.3390/w8050208.
Santinelli, C., 2015. DOC in the Mediterranean Sea. Biogeochemistry of Marine Dissolved Organic Matter, Second edition, pp. 579–608. https://doi.org/10.1016/B978-0-12-405940-5.00013-3.
Santinelli, C., Follett, C., Retelletti Brogi, S., Xu, L., Repeta, D., 2015. Carbon isotope measurements reveal unexpected cycling of dissolved organic matter in the deep Mediterranean Sea. Mar. Chem. 177, 267–277. https://doi.org/10.1016/j.marchem.2015.06.018.
Sempéré, R., Charrière, B., Van Wambeke, F., Cauwet, G., 2000. Carbon inputs of the Rhone River to the Mediterranean Sea: biogeochemical implications. Glob. Biogeochem. Cycles 14, 669–681.
Sheik, A.R., Brussaard, C.P.D., Lavik, G., Lam, P., Musat, N., Krupke, A., Littmann, S., Strous, M., Kuypers, M.M.M., 2014. Responses of the coastal bacterial community to viral infection of the algae *Phaeocystis globosa*. ISME J https://doi.org/10.1038/ismej.2013.135.
Shiller, A.M., Duan, S., van Erp, P., Bianchi, T.S., 2006. Photo-oxidation of dissolved organic matter in river water and its effect on trace element speciation. Limnol. Oceanogr. 51, 1716–1728. https://doi.org/10.4319/lo.2006.51.4.1716.
Sleighter, R.L., Hatcher, P.G., 2008. Molecular characterization of dissolved organic matter (DOM) along a river to ocean transect of the lower Chesapeake Bay by ultrahigh resolution electrospray ionization Fourier transform ion cyclotron resonance mass spectrometry. Mar. Chem. 110, 140–152. https://doi.org/10.1016/j.marchem.2008.04.008.
Spencer, R.G.M., Hernes, P.J., Aufdenkampe, A.K., Baker, A., Gulliver, P., Stubbins, A., Aiken, G.R., Dyda, R.Y., Butler, K.D., Mwamba, V.L., Mangangu, A.M., Wabakanghanzi, J.N., Six, J., 2012. An initial investigation into the organic matter biogeochemistry of the Congo River. Geochim. Cosmochim. Acta 84, 614–627. https://doi.org/10.1016/j.gca.2012.01.013.

Stedmon, C.A., Nelson, N.B., 2015. The optical properties of DOM in the ocean. Biogeochemistry of Marine Dissolved Organic Matter: Second Edition, pp. 481–508. https://doi.org/10.1016/B978-0-12-405940-5.00010-8.

Stedmon, C.A., Amon, R.M.W., Rinehart, A.J., Walker, S.A., 2011. The supply and characteristics of colored dissolved organic matter (CDOM) in the Arctic Ocean: Pan Arctic trends and differences. Mar. Chem. 124, 108–118. https://doi.org/10.1016/j.marchem.2010.12.007.

Urtizberea, A., Dupont, N., Rosland, R., Aksnes, D.L., 2013. Sensitivity of euphotic zone properties to CDOM variations in marine ecosystem models. Ecol. Model. https://doi.org/10.1016/j.ecolmodel.2013.02.010.

Vignudelli, S., Santinelli, C., Murru, E., 2004. Distributions of dissolved organic carbon (DOC) and chromophoric dissolved organic matter (CDOM) in coastal waters of the northern Tyrrhenian Sea (Italy). Estuar. Coast. Shelf Sci. 60, 133–149. https://doi.org/10.1016/j.ecss.2003.11.023.

Wagner, S., Fair, J.H., Matt, S., Hosen, J.D., Raymond, P., Saiers, J., Shanley, J.B., Dittmar, T., Stubbins, A., 2019. Molecular hysteresis: hydrologically driven changes in riverine dissolved organic matter chemistry during a storm event. J. Geophys. Res. Biogeosci. https://doi.org/10.1029/2018JG004817.

Ward, N.D., Keil, R.G., Medeiros, P.M., Brito, D.C., Cunha, A.C., Dittmar, T., Yager, P.L., Krusche, A.V., Richey, J.E., 2013. Degradation of terrestrially derived macromolecules in the Amazon River. Nat. Geosci. 6, 530–533. https://doi.org/10.1038/ngeo1817.

Weishaar, J., Aiken, G., Bergamaschi, B., Fram, M., Fujii, R., Mopper, K., 2003. Evaluation of specific ultra-violet absorbance as an indicator of the chemical content of dissolved organic carbon. Environ. Sci. Technol. 37, 4702–4708. https://doi.org/10.1021/es030360x.

Xie, H., Zafiriou, O.C., Cai, W.J., Zepp, R.G., Wang, Y., 2004. Photooxidation and its effects on the carboxyl content of dissolved organic matter in two coastal rivers in the southeastern United States. Environ. Sci. Technol. 38, 4113–4119. https://doi.org/10.1021/es035407t.

Yamashita, Y., Fichot, C.G., Shen, Y., Jaffé, R., Benner, R., 2015a. Linkages among fluorescent dissolved organic matter, dissolved amino acids and lignin-derived phenols in a river-influenced ocean margin. Front. Mar. Sci. 2, 92. https://doi.org/10.3389/fmars.2015.00092.

Yamashita, Y., McCallister, S.L., Koch, B.P., Gonsior, M., Jaffé, R., 2015b. Dynamics of dissolved organic matter in fjord ecosystems: contributions of terrestrial dissolved organic matter in the deep layer. Estuar. Coast. Shelf Sci. 159, 37–49. https://doi.org/10.1016/j.ecss.2015.03.024.

Yi, C., Pendall, E., Ciais, P., 2015. Focus on extreme events and the carbon cycle. Environ. Res. Lett. https://doi.org/10.1088/1748-9326/10/7/070201.

Zuijdgeest, A., Baumgartner, S., Wehrli, B., 2016. Hysteresis effects in organic matter turnover in a tropical floodplain during a flood cycle. Biogeochemistry 131, 49–63. https://doi.org/10.1007/s10533-016-0263-z.

Supplementary Information

TIME RESOLVED DATA UNVEILS THE COMPLEX DOM DYNAMICS IN A MEDITERRANEAN RIVER

Retelletti Brogi Simona [1,*], Balestra Cecilia[2], Casotti Raffaella[2], Cossarini Gianpiero[3], Galletti Yuri[1], Gonnelli Margherita[1], Vestri Stefano[1], Santinelli Chiara[1]

[1] *Istituto di Biofisica, CNR. Via G. Moruzzi, Pisa 56124, Italy*

[2] *Stazione Zoologica Anton Dohrn, Villa Comunale, Naples 80121, Italy*

[3] *Istituto Nazionale di Oceanografia e Geofisica Sperimentale (OGS), Borgo Grotta Gigante 42/C, 34010 Sgonico (TS), Italy*

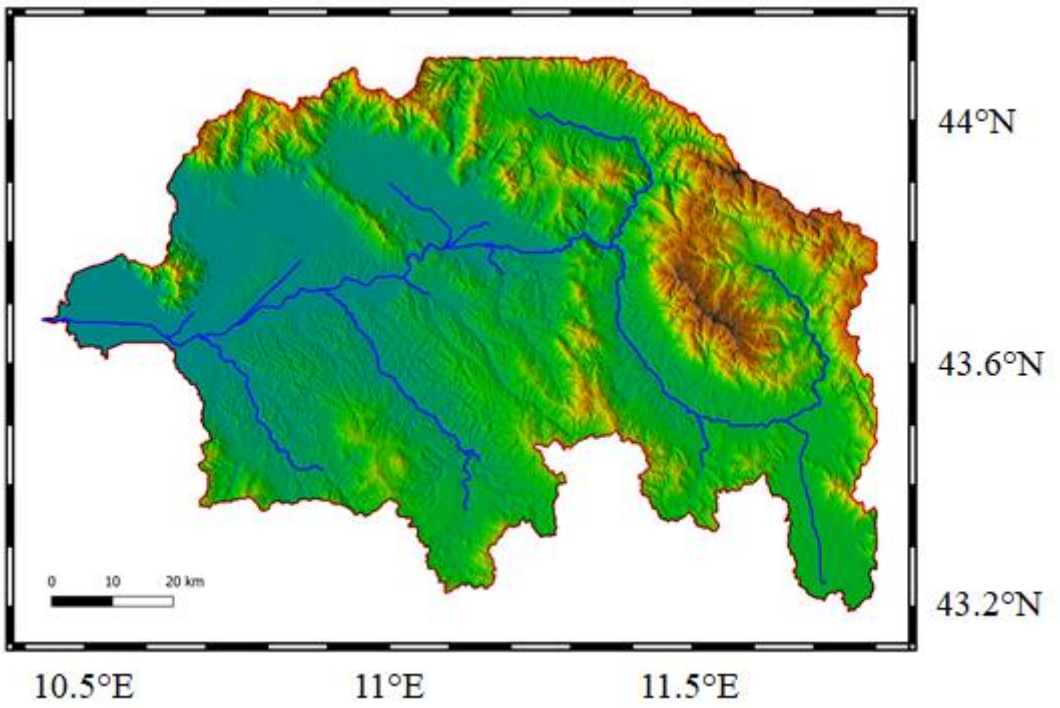

Figure S1 – Topography of the Arno River basin. The map was drawn by using the QGIS software.

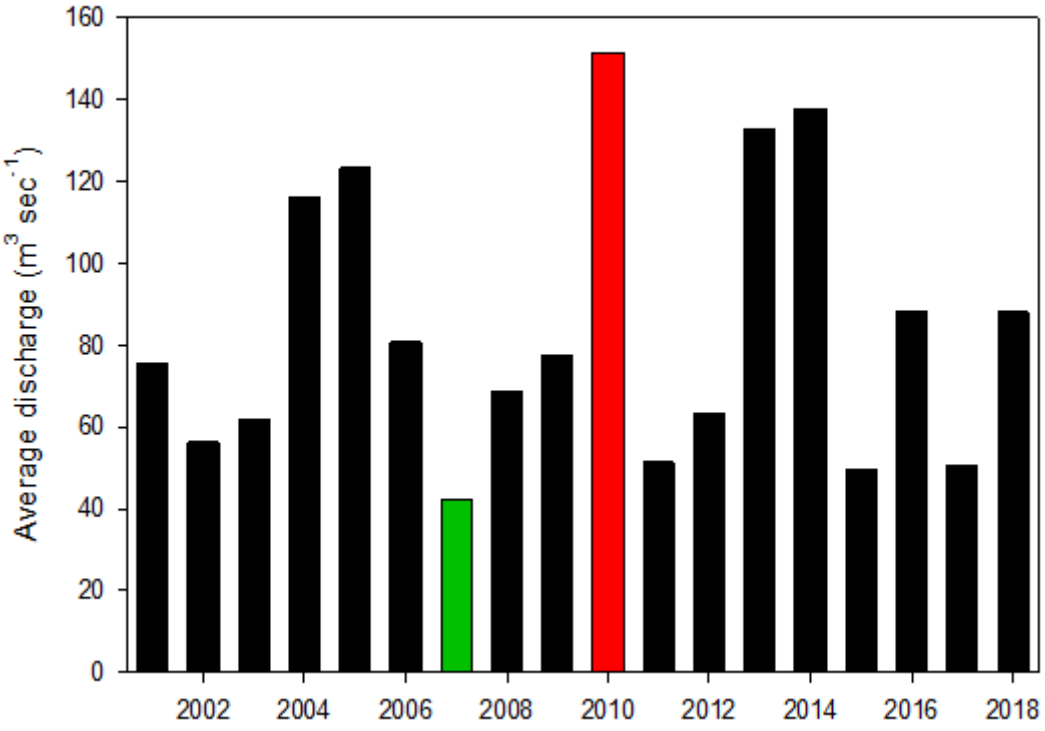

Figure S2 – Average discharge of the Arno River between 2001 and 2018. The green bar indicates the year with the lowest discharge, the red bar indicates the year with the highest discharge.

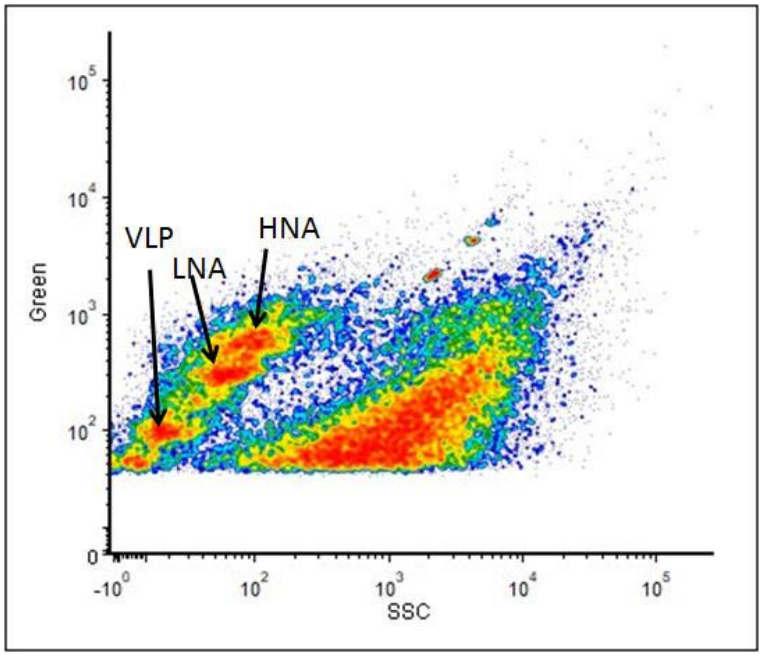

Figure S3 – Cytogram of Side Scatter (SSC) versus Green Fluorescence (Green) showing the Heterotrophic Prokaryote subgroup (High Nucleic Acid, HNA, Low Nucleic Acid, LNA), and the Virus-Like Particles (VLP).

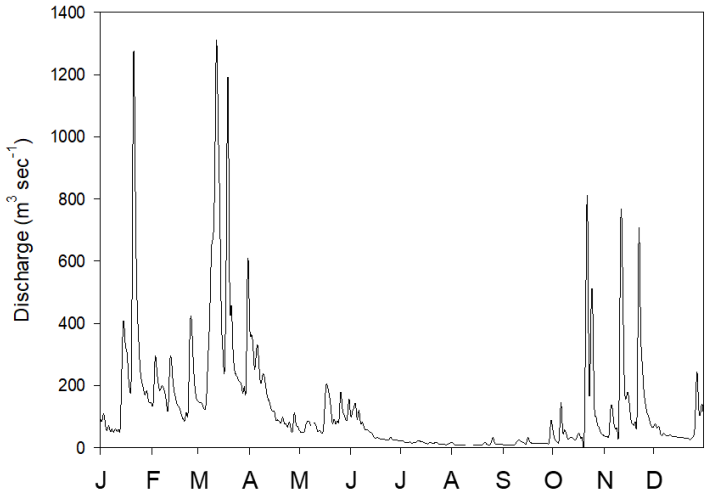

Figure S4 – Discharge of the Arno River in 2013. Data from the Regional Hydrological Service (www.sir.toscana.it).

Table S1 – Information on the environmental conditions during samples collection. Discharge, air temperature and precipitation data are available from the regional hydrographical service site (www.sir.toscana.it). Air temperature (maxima of the day) and precipitation information were taken from the closest monitoring station to the sampling location and are given as indicators of weather conditions.

Date (dd-mm-yy)	Time (hh:mm)	Discharge (m^3 sec^{-1})	Water Temperature (°C)	Air Temperature (°C)	Precipitation (mm)
30-01-14	09:30	355.8	7.5	12.8	56.6
03-02-14	09:45	530.7	9.7	14.1	1.8
05-02-14	10:00	402.5	8.8	12.6	10.2
11-02-14	10:05	1764.9	8.7	15.4	8.2
18-02-14	09:15	201.3	12.7	17.8	0
26-02-14	11:00	186.9	10.4	13.2	8.2
06-03-14	10:20	453.2	10.6	17.3	0
12-03-14	10:15	162.9	10.7	16	0
20-03-14	09:40	104.1	12.2	16.8	0
27-03-14	12:00	198.9	10.9	16.2	0
03-04-14	09:05	168.0	12.3	19.8	0
11-04-14	10:20	96.6	14.3	18.1	0
18-04-14	10:40	121.5	15.3	16.6	0
24-04-14	10:30	54.8	18.4	18.5	0
30-04-14	11:30	56.4	14.8	17.3	5.8
09-05-14	09:10	80.2	16.1	19.4	0
16-05-14	09:30	38.4	17.1	20.4	0
22-05-14	11:00	35.4	20.3	25.0	0
28-05-14	11:10	44.6	19.8	19.9	0
19-06-14	11:10	-	26.4	24.3	0
27-06-14	12:00	25.6	24.2	23.8	0
04-07-14	10:15	17.3	23.2	30.7	0
11-07-14	10:10	28.7	22.2	22.4	0
15-07-14	10:15	27.7	25.1	25.3	0
23-07-14	09:45	41.3	26.4	26.4	0.4
31-07-14	10:00	120.3	22.2	24.7	0
06-08-14	11:15	50.2	25.4	26.8	0
12-08-14	09:45	17.5	26.7	26.8	0
28-08-14	09:40	13.9	22.6	26.2	0
05-09-14	09:30	20.5	24.3	26.1	1.4
11-09-14	10:30	56.0	23.3	25.0	14.8
18-09-14	09:50	18.7	22.8	25.6	0
24-09-14	10:00	28.5	21	23.3	0
02-10-14	11:10	23.5	23	26.3	0
16-10-14	11:30	80.9	20.8	23.2	0.6
22-10-14	11:20	-	20.7	22.6	0
29-10-14	12:15	22.4	16.1	19.0	0
07-11-14	11:40	142.2	14	19.1	0.2
13-11-14	10:30	68.1	14.1	18.3	3.4
18-11-14	10:45	823.6	11.4	16.8	4.0
19-11-14	11:20	718.2	13	18.4	0.0

28-11-14	12:15	149.6	12.1	15.5	5.8
05-12-14	12:10	190.7	11.3	15.3	7.4
12-12-14	11:40	72.2	9	14.5	0
16-12-14	10:45	91.6	10.2	12.7	5.0
22-12-14	11:20	46.9	9.5	14.5	0.2
27-12-14	12:00	53.5	8.3	13.0	28.8
02-01-15	11:30	47.4	4.1	13.0	0
12-01-15	11:30	32.3	8	16.9	0
23-01-15	11:15	42.6	7.1	15.3	0
28-01-15	12:10	34.1	8.1	10.7	0
10-02-15	12:30	165.9	4.9	14.2	0
20-02-15	11:50	76.1	9.4	12.5	0
25-02-15	10:15	75.3	9.2	12.6	0.4
06-03-15	10:20	191.9	8.9	14.8	0
13-03-15	11:15	65.1	10	13.5	0
18-03-15	11:40	236.9	11.2	15.7	0
27-03-15	12:05	435.1	11.7	16.8	3.2
01-04-15	11:35	114.3	13.4	18.1	0
09-04-15	10:55	74.6	13.7	15.9	0
16-04-15	10:45	61.2	17.9	15.7	0.6
29-04-15	09:40	76.3	18.1	18.8	0
08-05-15	10:10	33.9	21.1	19.4	0
14-05-15	09:45	25.2	23.3	23.6	0
28-05-15	09:30	34.4	21.4	20.7	0
05-06-15	10:05	20.3	23.2	27.4	0
19-06-15	09:45	23.3	25.1	25.6	0
24-06-15	10:00	16.8	27	26.2	9.0
02-07-15	09:55	14.4	26.9	29.3	0
17-07-15	09:40	9.4	30.07	30.6	0
24-07-15	10:05	12.1	31.8	30.4	0
31-07-15	09:05	9.4	28.8	30.6	0.8
13-08-15	09:15	11.8	30.1	30.0	0
20-08-15	09:30	14.6	26.7	26.0	0
26-08-15	10:05	22.8	25	25.9	0
08-09-15	10:20	17.2	25.6	26.5	0
23-09-15	09:50	8.3	20.3	22.2	2.0
21-10-15	11:00	21.5	15.3	18.6	0
30-10-15	11:55	140.6	14.3	20.5	0
05-11-15	10:25	18.7	16.3	19.8	0
13-11-15	11:25	13.1	13.7	15.9	0
20-11-15	10:55	11.2	13.7	18.8	0.4
04-12-15	09:40	12.4	8.5	10.8	0
11-12-15	12:10	16.3	9.2	17.1	0
15-12-15	12:30	10.4	9.1	10.8	0

Table S2 - Comparison between the maxima of the excitation and emission spectra of the components identified in this study and those reported in the literature.

Components Ex/Em	**Similar components**	**Attribution**
C1	**Peak β** Parlanti et al., 2000	**Microbial humic-like**
<250(305)/408	**C2** Murphy et al., 2011	
	C4 Meng et al., 2013	
	C6 Maie et al., 2014	
	GoM2 Yamashita et al, 2015	
	C3 Lambert et al., 2016	
	C1 Ferretto et al., 2017	
C2	**Peak α** Parlanti et al., 2000	**Terrestrial humic-like**
<250(380)/494	**C2** Meng et al., 2013	
	C1 Maie et al., 2014	
	C2 Murphy et al., 2014	
	GoM4 Yamashita et al, 2015	
	C2 Lambert et al., 2016	
C3	**C3** Lapierre & Del Giorgio, 2014	**Terrestrial fulvic-like**
<250(350)/435	**Peak α** Parlanti et al., 2000	
	C360/456 Stedmon et al., 2011	
	C1 Maie et al., 2014	
	GoM1 Yamashita et al, 2015	
	C1 Lambert et al., 2016	
	C3 Ferretto et al., 2017	
C4	**Peak δ** Parlanti et al., 2000	**Protein-like**
280/355	**C5** Murphy et al., 2006	
	C3 Stedmon et al., 2011	
	C3 Hurr & Cho, 2012	
	C3 Meng et al., E2013	
	C5 Lambert et al., 2016	
	C2 Ferretto et al., 2017	
C5	**C1** Gonnelli et al., 2016	**Protein + PAH-like**
265/330	Li et al., 2013	
	C3 Nie et al, 2016	
	C6 Kothawala et al, 2013	
	Peak δ Parlanti et al., 2000	
	C3 Meng et al., 2013	
	C7 Maie et al., 2014	
	GoM5 Yamashita et al, 2015	